N71-19222

NASA CR-72811
ADL 71997

PRODUCTION OF OXIDE FIBERS BY A FLOATING ZONE FIBER DRAWING TECHNIQUE

by

J. S. Haggerty and W. P. Menashi

ARTHUR D. LITTLE, INC.

prepared for

NATIONAL AERONAUTICS AND SPACE ADMINISTRATION

NASA Lewis Research Center
Contract NAS 3-13479
L. Westfall, Project Manager

Requests for copies of this report should be referred to

National Aeronautics and Space Administration
Scientific and Technical Information Facility
P. O. Box 33
College Park, Maryland 20740

NASA CR-72811
ADL 71997

FINAL REPORT

PRODUCTION OF OXIDE FIBERS BY A FLOATING ZONE FIBER DRAWING TECHNIQUE

by

J. S. Haggerty and W. P. Menashi

ARTHUR D. LITTLE, INC.
15 Acorn Park
Cambridge, Massachusetts 02140

prepared for

NATIONAL AERONAUTICS AND SPACE ADMINISTRATION

February 1971

CONTRACT NAS 3-13479

NASA Lewis Research Center
Cleveland, Ohio 44135
L. Westfall, Project Manager

TABLE OF CONTENTS

FIGURES

TABLES

I. SUMMARY

A process was developed to produce oxide films with diameters between 0.002 to 0.015 inches (0.005 to 0.038 cm) for fiber reinforcement of metals subject to long-term elevated temperature service. Single crystal Al_2O_3 fibers in this diameter range were grown by a highly attenuated floating zone process.

Detailed heat transfer and zone shape analyses were made prior to initiation of fiber growth runs.

The dimensional limits for absolute and meta-stable molten zones between different size solid rods were analyzed for the first time. The process was shown to have many attractive features. Absolute stability could be achieved with thermally realizable dimensions and with high attenuation. Dimensional uniformity was enhanced because the tangent at the solidifying interface tended to parallel the growth direction. It was also shown that perturbations from the steady-state zone volume tend to damp out rapidly if the zone height remains constant.

Possible heat sources were assessed in terms of criteria that were felt important for the floating zone fiber growth process. Incandescent and CO_2 laser heat sources were identified as the best; although each had different advantages. Incandescent heaters were easily modified and most amenable to multifiber operations. The CO_2 laser had the greatest potential for producing fibers of high melting point materials. Fiber growth experiments were carried out with both types of heat sources and both heating techniques performed as anticipated on the basis of the analyses.

The room temperature and elevated temperature tensile strengths were shown to be highly sensitive to feed rod composition, ambient atmosphere and physical process conditions. Fibers of chromium-doped Al_2O_3 (ruby) were consistently stronger than high-purity Al_2O_3 fibers between 2080 and 2600°F (1140 and 1430°C).

It is suspected that the tensile strengths, which were somewhat lower than others reported for sapphire single crystal fibers, were limited by surface defects and unintentionally induced bending moments during tensile testing. The effect of surface treatments on tensile strengths were not studied in this program.

II. INTRODUCTION

The objective of this program has been to develop and use a liquid phase process for production of oxide fibers with diameters in the range of 0.002 to 0.015 inches (0.005 to 0.038 cm). These fibers are intended for fiber reinforcement of metals for long term service applications at temperatures from 2000°F (1093°C) to 2500°F (1371°C). The specific goals of the program were:

a. The production of oxide fibers with ultimate tensile strengths of 100,000 psi (6.9×10^8 N/m^2) or above at 2000°F (1093°C).

b. Length to diameter ratio should exceed 500. Spoolable lengths were desired; however, a minimum length of one inch (2.54 cm) was acceptable for small diameters.

c. The fibers were to have a cross sectional area equivalent to that of a circular cross section with diameters ranging from 0.002 inches (0.015 inches (0.038 cm) and a fiber length greater than 1 inch (2.54 cm).

d. The fibers need not be circular or single crystal; polygonal fiber shapes and polycrystalline fibers were acceptable.

e. The fibers were to be sufficiently non-friable to permit handling, similar to that in molding fiber-reinforced plastics.

f. Aluminum oxide was to be the primary oxide studied in this program; however, other oxides, such as ZrO_2 and HfO_2, were to have been studied at the recommendation of the contractor with the approval of the NASA Project Manager.

During the 12-month period that the contract was in effect, we have

a. analyzed the power requirements to produce a molten zone as well as the suitability of various heat sources for use with oxides,

b. analyzed the shapes and stability of the molten zones,

c. designed and constructed a fiber drawing apparatus which permitted satisfying the goals of the program.

d. produced and evaluated fibers.

The following report summarizes the results accomplished in these individual tasks.

III. DESIGN AND ANALYSES

A. Zone Shape and Stability Analysis

1. Zone Shape

As a first step in investigating the stability of zone shapes, we have made calculations for the equilibrium shapes of molten zones. In order to do this, it was first desirable to determine the relative magnitudes of the stresses which determine the equilibrium zone shape, with a view to simplifying the physical model and hence the mathematical treatment. The order of magnitude of the stresses produced by various physical phenomena which act on the zone area are:

Surface Tension	$\tau = \frac{\gamma}{r} \simeq 4 \times 10^3$ dynes cm^{-2}
Viscosity	$\tau = \frac{\eta v}{\ell} \simeq 10^{-4}$ dynes cm^{-2}
Dynamics	$\tau = \rho v^2 \simeq 4 \times 10^{-6}$ dynes cm^{-2}
Gravity	$\tau = \rho g \ell \simeq 4 \times 10^2$ dynes cm^{-2}

where

τ = stress, dyne cm^{-2}
v = velocity (10^{-3} cm sec^{-1} assumed)
γ = surface tension (400 dynes cm^{-1} assumed)
r = radius of zone (0.1 cm assumed)
ℓ = length of zone (0.1 cm assumed)
ρ = density of molten material (4 gm cm^{-3} assumed)
η = viscosity (10^{-2} poise assumed)
g = acceleration of gravity (approximately 10^3 cm sec^{-2})

It can be seen that viscous and dynamical effects are negligible, the gravitational pull has a marginal influence, and surface tension dominates.

The equation of equilibrium for the surface of the zone can therefore be represented by:

$$\gamma\left(\frac{1}{R_1} + \frac{1}{R_2}\right) = p_o - g\rho z \qquad (1)$$

where R_1 and R_2 are the principal radii of curvature of the surface of the zone, and z is the vertical coordinate, measured upwards, as shown in Figure 1. The constant p_o is the pressure at the origin. For analytical purposes, it is more convenient to introduce the arc length s and the angle ϕ of the slope of the equilibrium curve as shown in Figure 1 so that

$$\gamma\left(\frac{d\phi}{ds} + \frac{\sin\phi}{r}\right) = p_o - g\rho z \qquad (2)$$

and

$$\frac{dz}{ds} = \sin\phi \qquad (3)$$

$$\frac{dr}{ds} = \cos\phi \qquad (4)$$

Here r is the radial coordinate as shown in Figure 1.

If g is set equal to zero, Equation 2 simplifies to

$$\frac{d\phi}{ds} + \frac{\sin\phi}{r} = \frac{p_o}{\gamma} \qquad (5)$$

and it follows from Equations 4 and 5 that the shape of a zone will be unaffected by changes in the surface tension γ (the internal pressure p_o will change to compensate for changes in γ) and that zones of different scales will be similar. The zone shape will also be unaffected by the density of the material or the growth direction.

The following kinematic analysis of zone behavior was made to substantiate the assumed boundary conditions for a tendency of the melt surface to be parallel to the direction of growth at the solidifying interface. It was assumed that the height of the zone, the ratio of the feed rod and

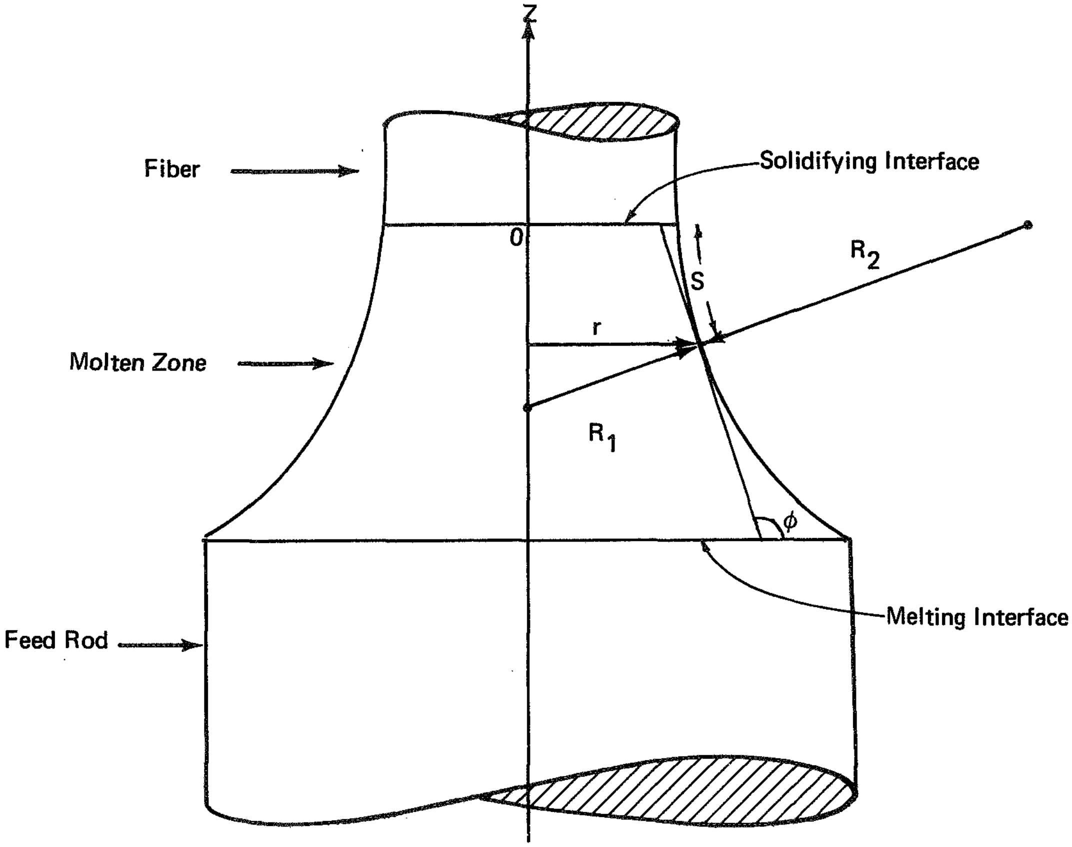

FIGURE 1 DEFINITION OF THE VARIABLES USED IN THE EQUATION FOR THE EQUILIBRIUM SHAPES OF FLOATING ZONE

fiber speeds, and the diameter of the feed rod are constant in this analysis. The feed rod and fiber are assumed to be equally dense.

Figure 2 shows a fiber being drawn from the molten zone before the steady state has been reached. In this figure

r_1 = radius at point of solidification

$\bar{r}_1$ = root mean square value of r_1 (determined by the relative speeds of the fiber and feed rod)

V = volume of molten zone

h = height of the molten zone

ϕ = angle of tangent at the top of the molten zone

r_2 = radius of feed rod

The vertical distance from an arbitrary point fixed on the fiber to the plane of solidification is denoted by ζ.

If it is assumed that the departure of r_1 from $\bar{r}_1$ is small so that

$$r_1 = \bar{r}_1 + \varepsilon \tag{6}$$

and ϕ is near 90°, the equation for the departure from the equilibrium radius is approximately

$$A \frac{d^2\varepsilon}{d\zeta^2} + B \frac{d\varepsilon}{d\zeta} + 2\pi \, \bar{r}_1 \varepsilon = 0 \tag{7}$$

Equation 7 may be solved (with a suitable choice of the origin of ζ) for ε to give

$$\varepsilon = \varepsilon_o^{-\frac{\zeta}{\delta}} \cos \frac{2\pi\zeta}{\lambda} \tag{8}$$

where

$$A \equiv \frac{\partial v}{\partial \phi} \tag{9}$$

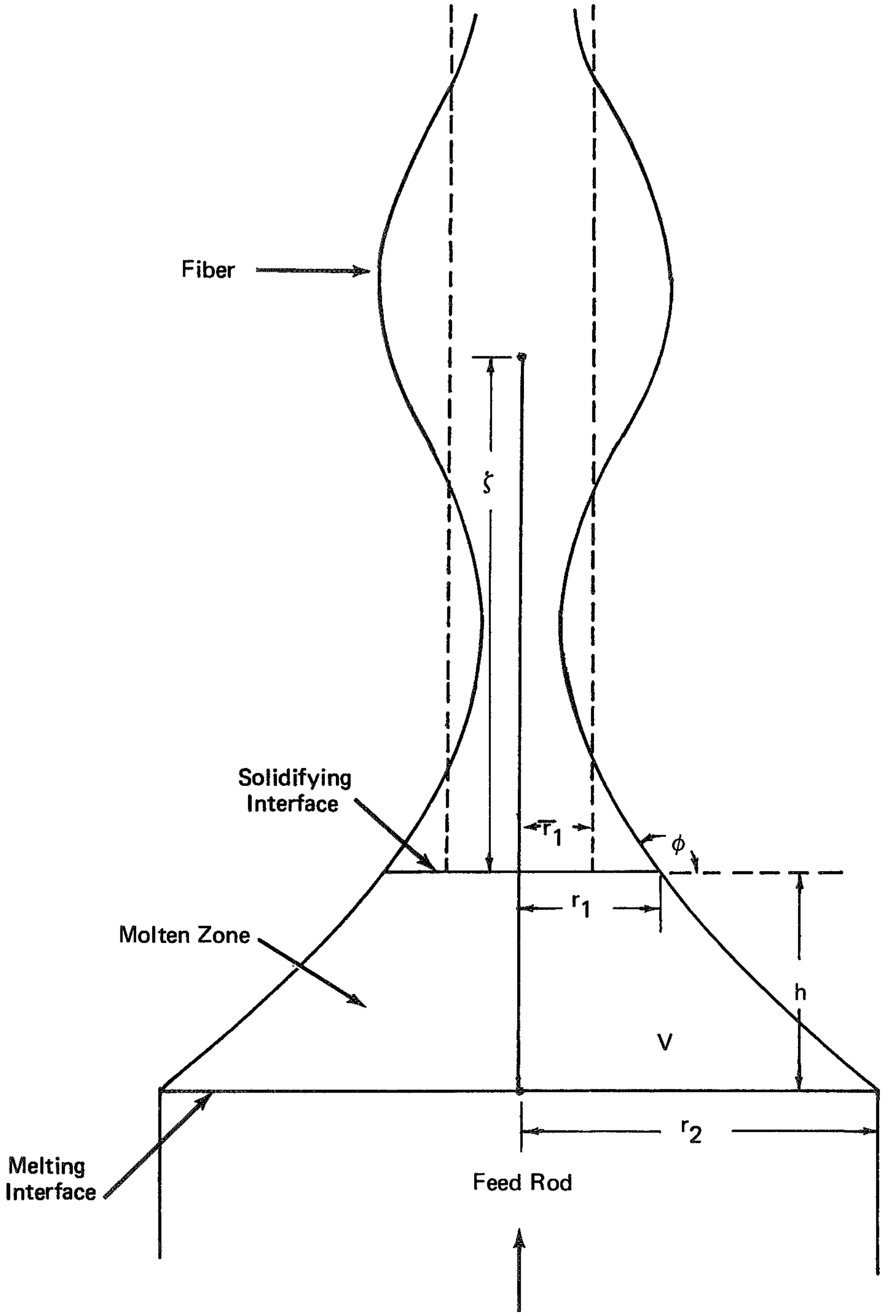

FIGURE 2 AN ILLUSTRATION OF THE VARIABLES USED TO ANALYZE THE EFFECT OF A PERTURBATION IN THE ZONE'S VOLUME ON THE DIAMETER OF THE FIBER

$$B \equiv \frac{\partial v}{\partial r_1} \tag{9}$$

and

$$\delta = \frac{2A}{B}$$

$$\lambda = \frac{4\pi\ A}{\sqrt{8\pi\ A\ \bar{r}_1 - B^2}} \tag{10}$$

To interpret Equation 8, it should be noted that A and B are always positive. Then, if λ is real (as it is in the numerical example given below), it is seen that the error in radius, ε, oscillates about zero with decreasing amplitude. In case λ is imaginary, the solution of Equation 7 takes the form of a sum of two exponentials of negative argument. In both cases, ε goes to zero and ϕ goes to 90° as the fiber is pulled. In other words, the tangent to the free surface of the molten zone at the freezing interface becomes vertical, and the diameter of the fiber settles down to a constant value.

In solving Equations 2, 3, 4 and 5 on the computer, only those shapes for which $\phi = 90°$ at $h = 0$ (vertical tangent) were considered. Figure 3 shows computed zone shapes for the case where gravity is ignored, i.e., where Equation 2 is replaced by Equation 5. The different zone shapes result from assuming different values of the curvature $1/R_2$ (see Figure 1), i.e., of $d\phi/ds$, at $h = 0$. The dashed parts of the two uppermost zone shapes, although physically possible, are not of practical interest. As pointed out above for the case of negligible gravity, the shapes shown in Figure 3 can be scaled up or down so long as the gravitational stress $g\rho\ell$ remains small compared with the surface tension stress γ/r.

A vertical line at some chosen radius in Figure 3 determines how the zone shape changes with zone height for a fixed ratio of feed rod to fiber diameter. Alternatively, the points of intersection of horizontal line across the zone contours determine the equilibrium zone shapes corresponding to various feed rod diameters for a fixed zone height.

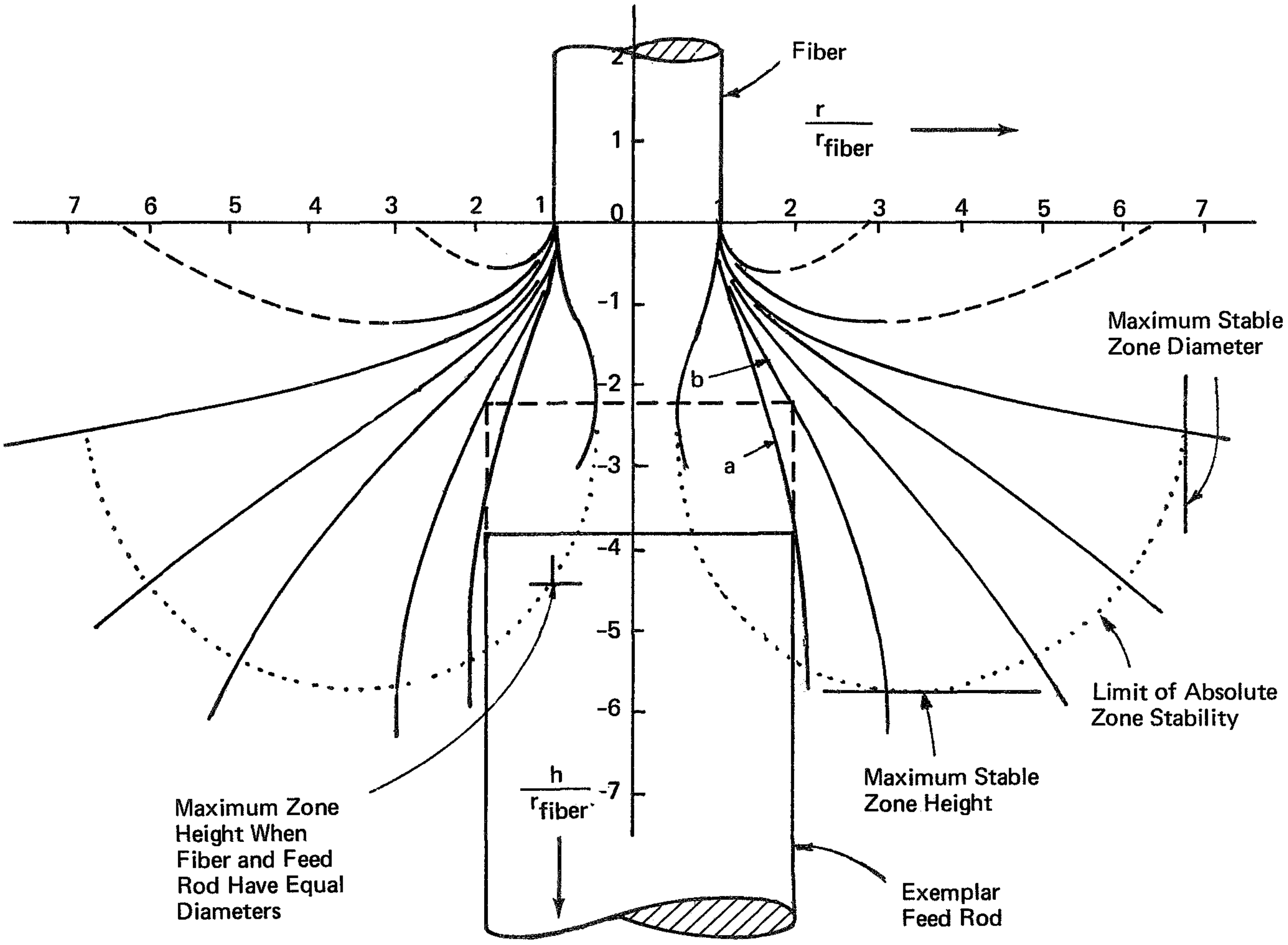

FIGURE 3 CALCULATED EQUILIBRIUM ZONE SHAPES PLOTTED IN TERMS OF THE ZONE HEIGHT (h) AND RADIUS (r) NORMALIZED TO THE FIBER RADIUS. THE CONTOURS "a" AND "b" REPRESENT POSSIBLE ZONE SHAPES FOR TWO ZONE HEIGHTS BETWEEN THE FIBER AND THE FEED ROD.

It is to be emphasized that there is a crucial difference (not properly brought out in the literature) between equilibrium shapes and stable shapes of zones. To be stable, the zone must be in an equilibrium shape, but not all equilibrium shapes are stable.

2. Zone Stability

Figure 4 shows, schematically, energy diagrams which illustrate the four possible different responses of zones to perturbation in shape. The surface energy E is proportional to the zone area A, while the amplitude of perturbation u is a measure of the hypothetical deformation of the equilibrium shape of the zone.

Figure 4a and 4b represent cases of absolute stability. In Figure 4a, it is energetically impossible to have the zone pinch off. In Figure 4b, absolute stability still prevails, but a meta-stable configuration (upper valley) exists in which the liquid has separated into two parts. In this case, it is possible for the zone to pinch off as a result of a perturbation large enough to surmount the energy barrier.

Figure 4c shows the case of a meta-stable zone shape separated by an energy barrier from an absolutely stable configuration in which the liquid is divided into two parts. In general, the energy barrier in this case is less than in the case of Figure 4b.

Finally, Figure 4d shows the case of complete instability of the zone. In this case, the equilibrium shape cannot exist physically.

The first step in investigating the zone stability quantitatively is to calculate the equilibrium shape of the liquid after hypothetical fission. After fission, the two parts of the zone form spherical caps on the two rods for the case where the distortion by gravity is negligible. If r_1 and r_2 are the radii of the rods, and h_1 and h_2 are the heights of the caps after separation, then the total volume of the two caps is

$$V_{caps} = \frac{\pi}{2}(r_1^2 h_1 + \frac{1}{3} h_1^3 + r_2^2 h_2 + \frac{1}{3} h_2^3) \qquad (11)$$

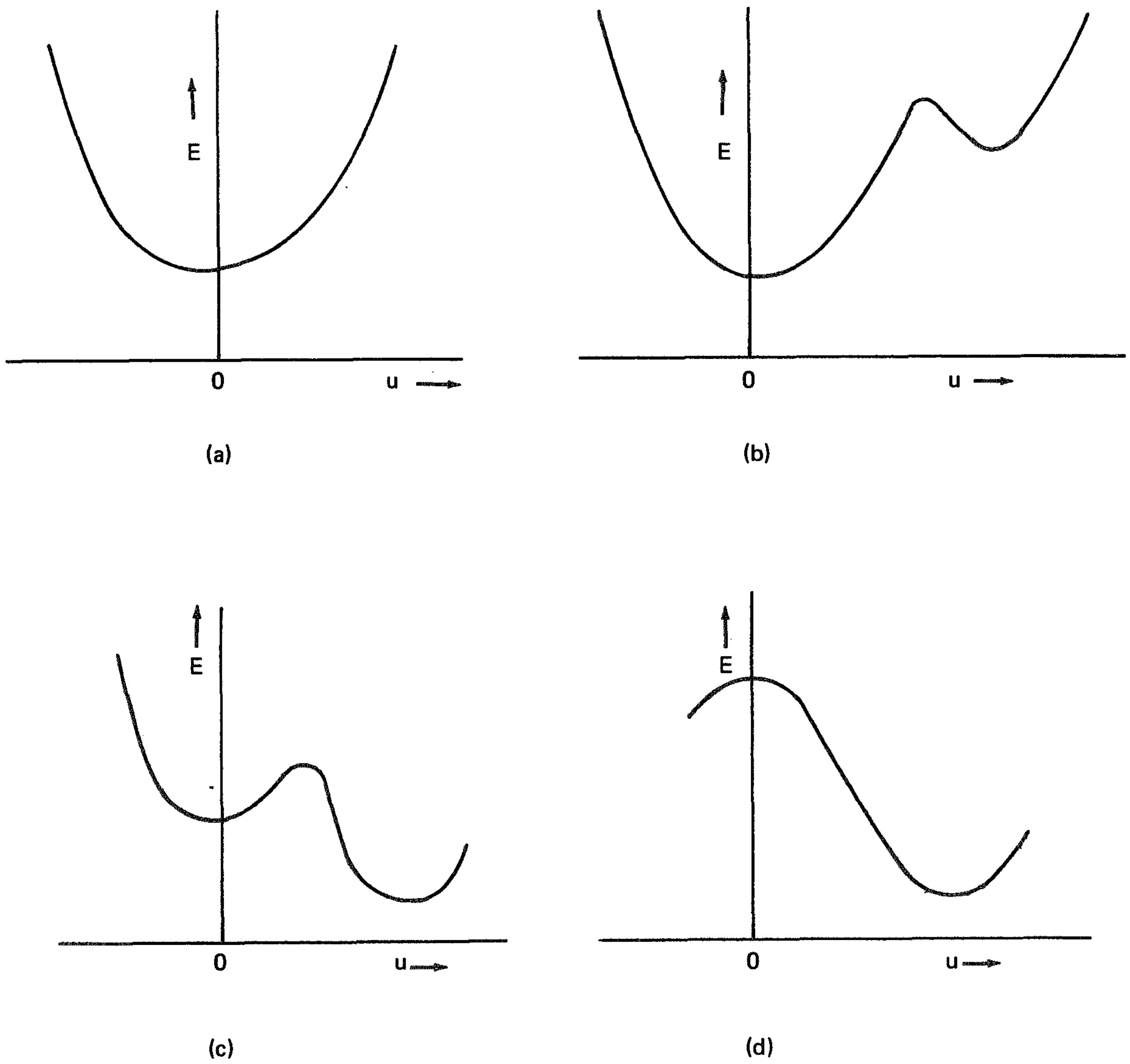

FIGURE 4 SCHEMATIC REPRESENTATIONS OF ZONE ENERGY (E) AS A FUNCTION OF A PERTURBATION (u) FROM THE EQUILIBRIUM SHAPE

and the total free surface area is

$$A_{caps} = \pi(r_1^2 + h_1^2 + r_2^2 + h_2^2). \tag{12}$$

The minimum surface energy of the two caps occurs when the liquid is partitioned in such a way that A_{caps} is a minimum, subject to the condition that V_{caps} is constant and equal to the volume of the equilibrium molten zone prior to separation. It was assumed in this stability analysis that these conditions were satisfied.

The ratio A_{caps}/A_{zone} is a measure of the stability of the zone. If this ratio is below unity, the zone is not absolutely stable (see Figure 4c). The dotted curves in Figure 3 show the locus of the limit of absolutely stable molten zones. If the zone height exceeds the indicated limit, the zone is not absolutely stable; whereas absolute stability is obtained for shorter molten zone heights.

It is apparent from Figure 3 that absolutely stable zones can be achieved only so long as

$$\frac{r_{rod}}{r_{fiber}} \leq 6.7 \tag{13}$$

and

$$\frac{h}{r_{fiber}} \leq 5.7 \tag{14}$$

Figure 5 shows how the stability factor A_{caps}/A_{zone} varies with the ratio of zone height to fiber radius, h/r_{fiber}, for a number of different values of the attenuation ratio, r_{feed}/r_{fiber}. It is seen that for higher attenuation ratios the stability factor is close to 1 and approaches unity quite gradually. All the curves, when extended, intersect the horizontal at or before the point marked A in Figure 5.

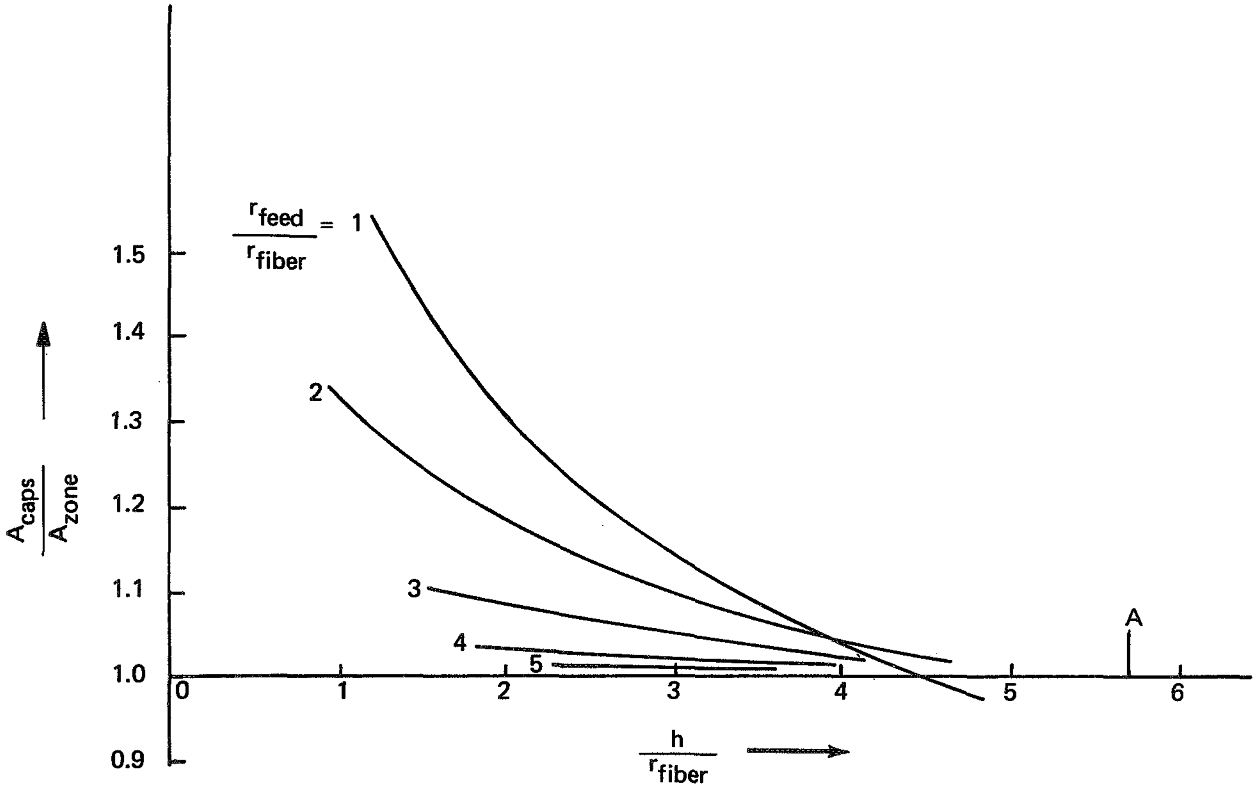

FIGURE 5 ZONE STABILITY AS A FUNCTION OF ZONE HEIGHT FOR VARIOUS ATTENUATION RATIOS

The surface area of the zone was calculated as a function of the amplitude of a perturbation to investigate the character of zone stability in more detail. The form of the perturbation was assumed to be such that the volume of the zone remained unchanged. A radial perturbation which satisfies this criterion is

$$r' = r\left(1 + u \sin \frac{2\pi z}{h}\right)^{1/2} \tag{15}$$

The perturbed zone area A' is given by

$$A' = \int 2\pi r' \, ds' \tag{16}$$

or

$$A' = \int_0^h 2\pi r' \sqrt{1 + \frac{dr'}{dz}^2} \, dz \tag{17}$$

In general, Equation 17 cannot be evaluated analytically. However, the case in which the two rods have equal radii is one special case which is tractable. The general case must be treated numerically.

From Equations 15 to 17, it can be shown that the perturbed area of a molten zone between equal diameter rods is given by:

$$A' = 2\pi \int_0^h r\left[1 + u \sin\left(\frac{2\pi z}{h}\right) + \left(\frac{\pi r u}{h}\right)^2 \cos^2\left(\frac{2\pi z}{h}\right)\right]^{1/2} dz \tag{18}$$

and from Equation 18 that

$$\left(\frac{d^2A'}{d\,u^2}\right)_{u\,=\,0} = \pi r^3 h \left(\frac{\pi^2}{h^2} - \frac{1}{4r^2}\right) \tag{19}$$

If the second derivation is positive, the zone is either absolutely stable or meta-stable as shown in Figure 4a, 4b, or 4c; whereas, if it is negative, the zone is unstable as shown in Figure 4d.

The condition for stability for the special case of equal diameter rods is that

$$\frac{h}{r_{fiber}} < 2\pi \tag{20}$$

This same solution for the stability limit between equal diameter cylinders has been derived by another technique.(1) This height limit for stability exceeds that derived for absolute stability between equal diameter cylinders indicated in Figure 3

$$\frac{h}{r_{fiber}} < 4.5 \tag{21}$$

From this, it is concluded that meta-stability probably extends the working region some significant distance beyond the limit shown by the dotted curve in Figure 3. The general solution for the meta-stable limits and the height of the energy barrier for various zone heights and attenuation ratios required numerical evaluation of Equation 16 and was not undertaken.

B. Selection of Heating Methods for Fiber Drawing

1. Selection Criteria

The following criteria were used to evaluate possible heat sources for the floating zone fiber growth process.

- Maximum Temperature -- The heating method must have been capable of melting ceramics such as alumina, spinel, or zirconia. The objective of the program was to have the capability of melting oxides with melting points in excess of 5400°F (3000°C).

- Temperature Stability -- An acceptable heating method must have had both long and short term temperature stability. Temperature stability could be achieved either by active control of the heating method or by the inherent long and short term stability of the heating method itself.

- Molten Zone Height -- An acceptable heating method must have been capable of producing a molten zone with dimensions of the order of 0.040 inches (0.1 cm). Variation of the zone height should not require major equipment changes.

- Axial Temperature Distribution -- The heating method must have been capable of producing a desired temperature distribution in both the feed and drawn fiber. The distribution will generally be determined by the properties of the fiber and the system geometry; however, the heating method should not severely resitrict possible temperature gradients.

- Circumferential Uniformity -- The heating method must have been promoted circumferential uniformity of the temperature distribution in the solid feed rod, molten zone and pulled fiber.

- Temperature Control Potential -- The heating method must have been readily adaptable to automatic temperature control by conventional methods, both in the laboratory for development, and ultimately for production use.

- Visibility -- The heating method must have permitted viewing the sample with optical pyrometers, optical instruments, or photographic equipment. Visual observation capability was desirable but not essential.

- Environmental Restrictions -- The heating method must have permitted use of a broad range of ambient gases at pressures ranging from high vacuum to over one atmosphere.

- Flexibility -- The heating method must have permitted changes in sample geometry, temperature, temperature distribution and sample environment without extensive equipment modifications.

- Potential for Multiple Fiber Use -- The heating method must have been adaptable to drawing of several fibers without requiring replication of the entire system. Preferably, one heating unit should suffice for from 1 to 10 fibers with uniform quality of temperature and other important parameters.

- Availability -- The heating method should be available for laboratory use at ADL, easily assembled from existing or readily fabricated parts, or available on a rental basis.

- Cost — The cost of the heating method must not have been excessive, both for the development of production model systems.

2. Techniques Investigated

Four types of thermal radiation heating and three direct heating methods were considered:

- Resistance elements which surround the sample are heated by passage of direct or alternating current; heat transfer to the samples is primarily by thermal radiation.
- RF heated elements which surround the samples; heat transfer to the samples is primarily by thermal radiation.
- Thermal imaging techniques with radiation sources such as carbon arcs or xenon lamps are used to heat the samples.
- Lasers, either continuous or pulsed, are used to heat the samples.
- An electron beam heating is used to heat the samples.
- Gas discharge heating is used to heat the samples.
- Direct RF coupling to the heated ceramic is used to bring the sample to the melting point.

3. Comparison of Heating Methods

It was concluded on the basis of this review that infrared heating (resistance and rf) and laser heating were the two techniques best suited to this floating zone fiber growth process. The results of this study are summarized qualitatively in Table I.

The infrared heating techniques were considered to be generally more flexible and controllable than the others considered, and have the best potential for multi-fiber processes. It became clear, however, that there were no commonly available materials that can be used as incandescent heaters for oxides with melting points in excess of 5400°F (3000°C). Graphite and tungsten could be used for Al_2O_3, and they could probably be used, but with short and uncertain life, for spinel ($MgO \cdot Al_2O_3$ and ZrO_2). More refractory materials, e.g., TaC and HfC, would be prohibitively expensive to fabricate

TABLE I

COMPARISON OF HEATING METHODS

Method	Maximum Temperature	Temperature Stability	Molten Zone Height	Circumferential Uniformity	Axial Temperature Distribution	Temperature Control Potential	Visibility	Environmental Restrictions	Flexibility	Potential for Multiple Fiber Production	Availability and Cost
Infrared Heating -- Resistance Elements	$< 3000^{\circ}C$, depending upon material and environment limitations	Good, both short and long term	Can be varied by using different elements	Good	Determined by heater-shield design and materials properties--flexibility of design	Good	Fair	Vacuum, inert or reducing environment	Systems easily changed or modified	Good	Good
Infrared Heating -- R.F. Heated Elements	$< 3000^{\circ}C$, depending upon material and environment limitations	Good, both short and long term	Can be varied by using different elements. R.F. coils also effect heat transfer	Good	Determined by heater, shield and susceptor design and materials properties. Flexibility restricted by rf coils and susceptor	Good	Fair--Poor	Vacuum, inert or reducing environment, some pressure ranges not feasible.	Systems easily changed or modified	Good	Good
Infrared Heating -- Thermal Imaging	$>3000^{\circ}F$ depending upon source and optical system	Fair to poor in intermediate and long term	Difficult to focus to small sizes	Poor because of image directionality and shadowing	Poor because of source flux inhomogenieties	Fair -- Poor	Good	None	Cumbersome, expensive optical system reduces flexibility	Poor	Good
Laser Heating	$> 3000^{\circ}F$, limited in practice only by sample size, geometry and available power	Relatively good; typical laser life 1000 hours	Can be controlled by focusing and adjusting optics	Can be good with properly designed optics or use of multiple lasers	Good	Good	Good	None	Relatively flexible within power limitations	Poor	Good
Electron Beam	$> 3000^{\circ}C$, depend-only on beam power	Poor, depends upon conductance of sample and feedback system	Can be controlled by focusing, but unstable	Poor because of directionality	Poor because of lack of stability	Poor	Good	Requires gas pressures below 10^{-4} torr	Relatively flexible to different size samples	Poor	Fair
Gas Discharge	At least $2410^{\circ}F$.	Probably good	Not easily controlled, fixed by cathode geometry and discharge parameters	Good	Probably poor because of discharge surrounding molten zone	Probably good	Poor	Gas environment ≈ 1 torr	Sample sizes easily changed, may require changes in electrode configuration	Poor	Fair

into heaters. It was suggested that the fiber growth apparatus be designed to employ this type of heating and that the experimental program be initiated with resistance heated filaments. The experience gained in handling the fibers, with zone attenuation and stability and fiber testing will prove valuable for any heating technique.

To take full advantage of the crucibleless floating zone process and to make possible the growth of oxide fibers with melting points in excess of 5400°F (3000°C), it was suggested that experiments should be initiated with CO_2 laser heating. Arrangements were made to rent a 10 watt CW CO_2 laser which was used for a series of preliminary laser-heated fiber growth experiments.

C. Infrared Heating -- Thermal Design Analysis

Detailed thermal analyses were made to confirm the feasibility of using an infrared heating source to melt feed stock and draw thin fibers, as well as to provide information required for the design of the heater. Although most of the analyses were conducted parametrically, materials, dimensions, and boundary conditions were selected which were representative of the projected operating system both to add realism and to establish practical limits of feasibility. Aluminum oxide was selected as a model system.

The objectives of the analyses were to answer the following questions for a fiber drawing process in which an incandescent heater surrounds the feed stock:

- What is the heater temperature and power required to form a molten zone.
- What is the thermal stability of the molten zone.
- What is the temperature distribution in the feed stock and fiber.
- What are the effects of "clearance" between the heater and feed rod.
- What are the effects of radiation shields.

1. The Simplified Model for Analysis

The model for thermal analysis is shown in Figure 6.

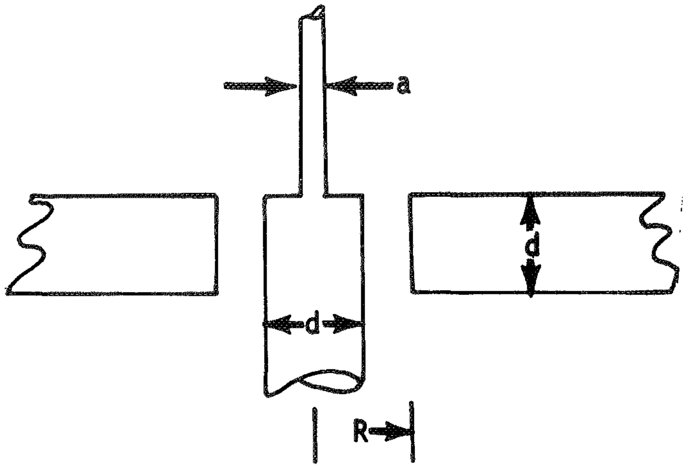

Figure 6. Definition of Parameters Used in Thermal Analyses

In the initial analysis, it was assumed that the cavity in the heater would be cylindrical, of radius R and length d equal to the diameter of the feed rod.

2. Heater Power and Temperature Requirements

As a first estimate of the power required to form a molten zone of length d, it was assumed that the gap between the heater and the feed rod was small ($R \simeq d/2$), that the fiber had a much smaller diameter than the feed rod ($a \ll d$), and that the losses from the molten zone were by conduction along the feed rod and by radiation from the end of the molten zone. When the feed rod is heated, a steady state will be reached in which the heat absorbed by the rod equals the losses from the rod as follows:

$$q \text{ absorbed} = \pi d^2 \sigma (T_H^4 - T_R^4) \left[\frac{1}{\frac{1}{\alpha_R} + \frac{1}{\varepsilon_H} - 1} \right] \qquad (22)$$

and

$$q \text{ loss} = \frac{\pi d^2}{4}\left[\varepsilon_R \sigma T_R^4 + \sqrt{\frac{4hk_R}{d}}\left(T_R - T_0\right)\right] \tag{23}$$

where ε_R, α_R and ε_H are the emittance of the rod, absorptance of the rod, and emittance of the heater, respectively, T_H, T_R, and T_0 are the heater, rod, and ambient temperatures, respectively, h is a heat transfer coefficient (convection plus radiation) from the rod and k_R is the thermal conductivity of the rod. If convection losses are negligible compared to radiation

$$h = \frac{\varepsilon_R \sigma (T_R^4 - T_0^4)}{(T_R - T_0)} .$$

Combining the equations,

$$\sigma(T_H^4 - T_R^4)\left[\frac{1}{\frac{1}{\alpha_R} - \frac{1}{\varepsilon_H} - 1}\right] = \frac{1}{4}\left[\varepsilon_R \sigma T_R^4 + \sqrt{\frac{4\sigma\varepsilon_R(T_R^4 - T_0^4)k_R(T_R - T_0)}{d}}\right] \tag{24}$$

which relates the required temperature and properties of the heater to the properties of the ceramic feed rod.

Literature data on molten alumina indicate that the spectral emittance varies between about 0.86 and 0.93 at wavelengths of 0.65 and 2.4 microns. Conflicting data are present in the literature for solid alumina. Using literature data for optical constants in the region from 0.5 to 7 microns, we have estimated the emittance and absorptance of aluminum oxide, both solid and molten, over the temperature range of 500 to 3850°F (260 to 2120°C). For small rod and fiber sizes the emittance of aluminum oxide will vary with the sample diameter. Table II gives our estimates of emittance values.

TABLE II

EMITTANCE OF ALUMINUM OXIDE AT DIFFERENT TEMPERATURES

Temperature		d = 0.1 inches (0.254 cm)	d = 0.01 inches (0.0254 cm)
°F	°C		
Molten		>.75	>.15
3600	1980	0.11	0.03
2700	1485	0.21	0.07
1800	980	0.42	0.18
900	480	0.80	0.55

It is important to note the emittance is relatively high at low temperatures because the aluminum oxide is almost opaque at long wavelengths. The emittance decreases as temperature increases because of its transparency and then increases sharply at the melting point.

Equation 24 gives two solutions for the rod (zone) temperature with a constant heater temperature because of the difference between the solid and liquid emissivities. Therefore, the heater must be heated to a higher temperature to initiate melting than is required to maintain a molten zone. Superheating is required to insure stability.

a. Graphite Heater

The minimum heater temperature to just maintain a molten zone of Al_2O_3 with a graphite heater is 4350°F (2400°C). A heater temperature of approximately 4530°F (2500°C) is probably required to insure stability. Under these conditions a 0.1 inch (0.254 cm) diameter feed rod would adsorb approximately 22 watts.

b. Tungsten Heater

If tungsten were used as the heater, a higher heater temperature would be required than with graphite because of its low emittance. Assuming an emittance of 0.3, the required heater temperature to maintain

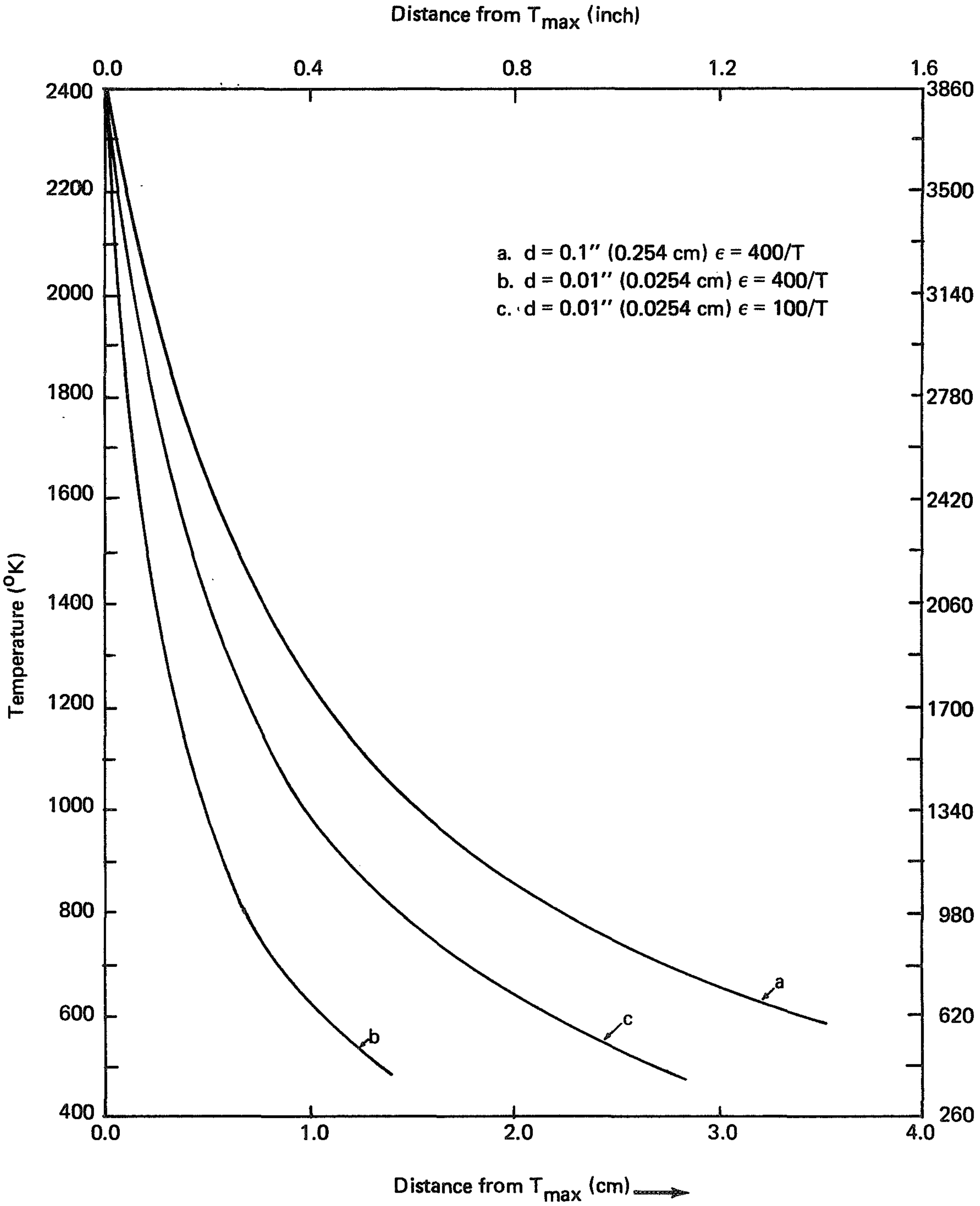

FIGURE 7 TEMPERATURE DISTRIBUTION ALONG THE FEED ROD AND FIBER

molten Al_2O_3 zone is approximately 5075°F (2800°C). This is a very high operating temperature for tungsten and suggests that it may not be suitable material as graphite.

3. Temperature Distribution in Feed Rod

The temperature distribution from the molten zone to the cold end of the rod is found from the solution of the following equation:

$$\pi r^2 k_R \frac{d^2 T_R}{dx^2} = 2\pi r \left[\varepsilon_R \sigma (T_R^4 - T_0^4) + h(T_R - T_0) \right] \tag{25}$$

where r is the radius of the feed rod and h is the convection coefficient at the rod surface. As a first approximation, because T_R is much larger than T_0 in the region near the molten zone and h is small, Equation 25 reduces to:

$$\frac{d^2 T_R}{dx^2} = \frac{2}{k_R r} \varepsilon_R \sigma T_R^4 \tag{26}$$

In the temperature region of interest (450 to 3720°F, 230 to 2050°C) the emittance can be approximated as $\varepsilon_R = \frac{400}{T}$, and the solution of Equation 26 is

$$x = \sqrt{\frac{k_R r}{200\sigma}} \left[\frac{1}{T_R} - \frac{1}{T_{R_{max}}} \right] \tag{27}$$

where $T_{R_{max}}$ is the temperature at the molten zone. Calculated temperature distributions in 0.01 inch (0.0254 cm) and 0.10 inch (0.254 cm) diameter Al_2O_3 rods are shown in Figure 7.

The calculated temperature distribution in an 0.1 inch (0.254 cm) diameter feed rod is given by curve a. Curve b represents the temperature distribution in an 0.01 inch (0.0254 cm) diameter fiber assuming the same emissivity as the feed rod ($\varepsilon = 400/T$). It was shown previously, Table II, that the emittance of the fiber is lower than the rod by a factor of two to four depending on temperature. Curve c is the temperature distribution calculated assuming an emittance of $\varepsilon = 100/T$. The actual temperature gradient for the fiber will probably be between curves b and c. The initial temperature gradient in the fiber will be between two to three times higher than in the feed rod. The relatively steep temperature gradient in the fiber is useful since it permits high solidification rates.

For the Al_2O_3 example with zero clearance between the heater and feed rod, it was found that the heat transferred by conduction down the feed rod is about twice the amount lost by radiation from the end of the molten zone.

4. Effects of Clearance Between Heater and Feed Rod

The preceding results were evaluated for a system in which the gap between the feed rod and the heater was small. In practice, clearance is required between the heater and the molten zone and the effect of the gap between the heater and the feed rod was evaluated.

For the case where the clearance between the heater and the feed rod is equal to the radius of the feed rod (radius in heater - 2 x feed rod radius), it was found that the equilibrium graphite heater temperature to just keep Al_2O_3 at its melting point is 4920°F (2730°C) and the power absorbed by the molten zone is about 32 watts for a 0.1 inch (0.254 cm) diameter feed rod. In this case the heat losses from the zone are about 60% by radiation and 40% conduction down the feed rod. If the gap were decreased to only one half the radius of the feed rod (radius in heater = 1.5 x feed rod radius), the heater temperature would be about 4685°F (2585°C) or about 360°F (200°C) higher than if no gap were present. A tungsten heater would have to be operated at a significantly higher temperature because of its lower emittance. Thus, it is desirable to reduce the gap as much as possible. Clearly, the temperature distribution in the feed rod and pulled fiber will also be affected by the gap width. In general, the larger the gap, the smaller the axial temperature gradient adjacent to the molten zone.

5. Temperature Distribution in Molten Zone

In the preceding analyses, we have considered that the temperature in the molten zone would be uniform. This is clearly not the case because of different heat losses from each end of the rod as well as varying view of the heater from different parts of the molten zone. A detailed analysis of the temperature distribution in the molten zone is complex, particularly if the geometry of the zone is not well defined. The temperature will be a maximum near the centerline of the heater and decrease gradually until the edges of the heater and then more rapidly outside the zone adjacent to the heater. In an actual system, it may be desirable to confine the molten zone to within the heater boundaries so that too much superheat will not be achieved at the center of the molten zone. For example, the center of the molten zone would be superheated by about 540°F (300°C) for a system in which the diameter of the feed rod were equal to the thickness of the heater, the gap between the heater and the rod were equal to the radius of the rod and the molten zone extended to the ends of the heater. Reducing the gap reduced superheating.

6. Effect of the Feed Rod and Heater Size

The emittance of the molten zone decreases faster than the emittance of the solid feed rod as their sizes are reduced. Therefore, the fraction of the heat lost from the zone by conduction increases as diameter decreases. We estimate that a graphite heater temperature of approximately 4670°F (2580°C) would be required to melt a closely coupled 0.05 inch (0.125 cm) diameter Al_2O_3 rod compared with 4350°F (2400°C) required for a 0.1 inch (0.25 cm) rod. Because the exact shape and surface to volume ratio of the zone strongly influences the absorption and loss terms, it was not considered useful to make more elaborate calculations.

D. Fiber Growth Apparatus

Three distinct pieces of fiber growth apparatus were constructed and used successfully during the one year program. The first used a rf heated IR source in a modified ADL-MP Crystal Growing Furnace. The second used a 10 watt CO_2 laser heat source. The third used a resistance heated IR source in a furnace chamber constructed specifically for this program. The fiber growth experiments carried out in the first two were limited in scope to demonstrating feasibility and testing analyses.

1. RF heated - IR Source; Modified MP Furnace

A series of preliminary fiber growth experiments were carried out in an ADL-MP Crystal Growing Furnace, Figure 8, using a rf power supply. The drive train to the pulling heads was modified to permit continuously adjustable relative rates of shaft travel so that smooth, attenuated fiber growth was possible. As normally constructed, the upper and lower shaft of the Crystal Growing Furnace travel at the same rates when both are engaged. This modification was accomplished by inserting a continuously adjustable gear box (ball and disk type) into the lower pulling head drive. The unit could be adjusted so that the lower shaft traveled at lower, equal or higher rates than the upper shaft.

In the first installation of the continuously adjustable gear box, flexible drive shafts were used to connect the main gear box to the pulling head. It was observed that the spring shafts had a tendency to wrap up and transmit an interrupted motion to the lower head. This was reflected in the fibers as a non-uniform diameter. These flexible shafts were replaced with torsionally more rigid drive shafts which contained universal joints to compensate for misalignment. This latter modification of the drive train functioned properly, although one must always be alert to the possibility of slippage in a non-positive gear box of this type.

Two rf coil-heater assemblies were used in this series of experiments. The first, shown schematically in Figure 9, was used in the first seven runs; and the second, Figure 10, was used in runs eight through forty-one.

The graphite heater disks in the first assembly were supported on graphite legs to minimize the contact area between the heater and the insulating BN support (High Purity Grade, Carborundum Company). This coil-heater assembly was not well suited to usage in either argon or vacuum atmospheres due to the high electrical potential between the rf coil and the disk heater. Frequent arcing occurred when operated under these conditions.

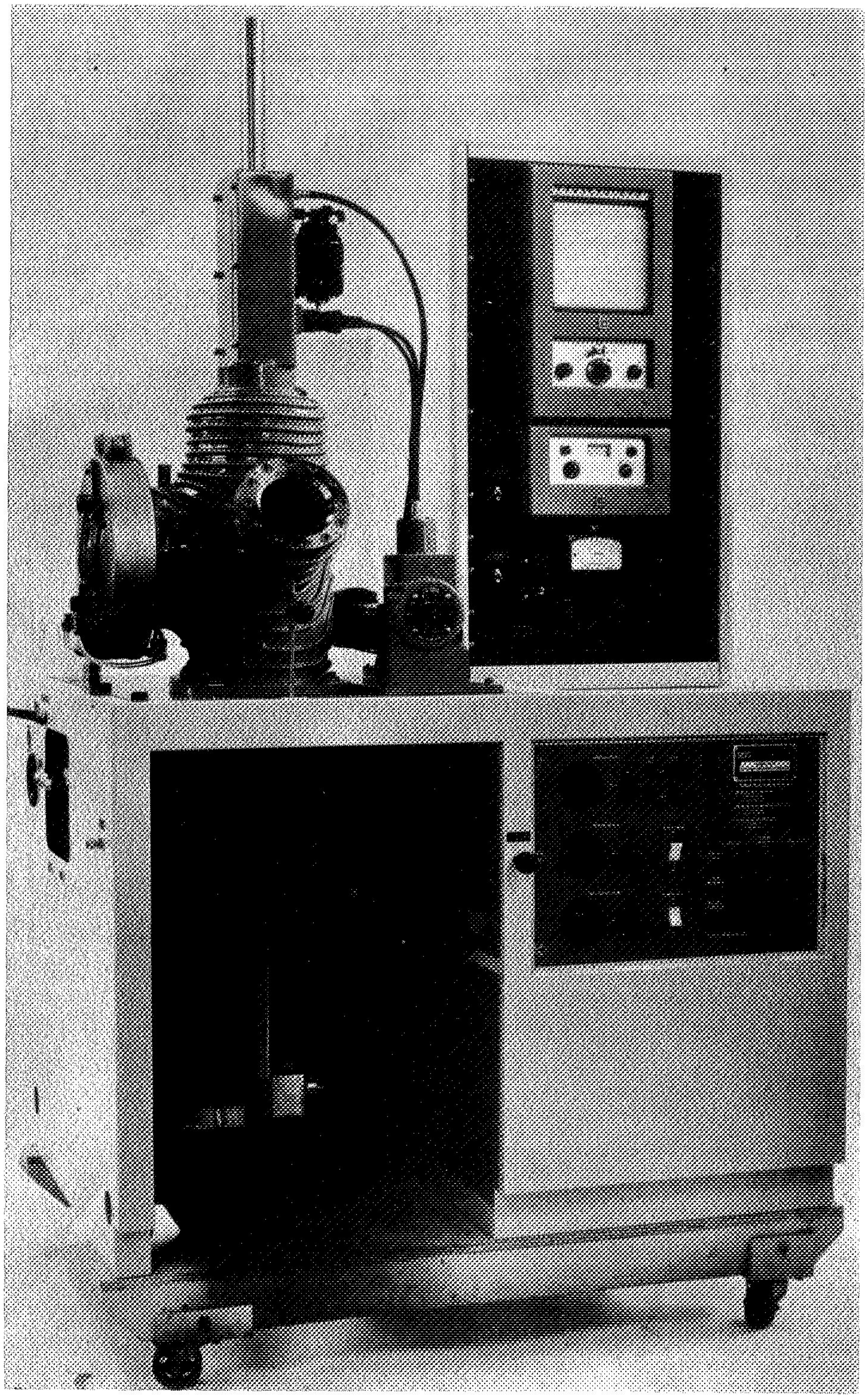

FIGURE 8 ARTHUR D. LITTLE, INC., MP CRYSTAL GROWING FURNACE

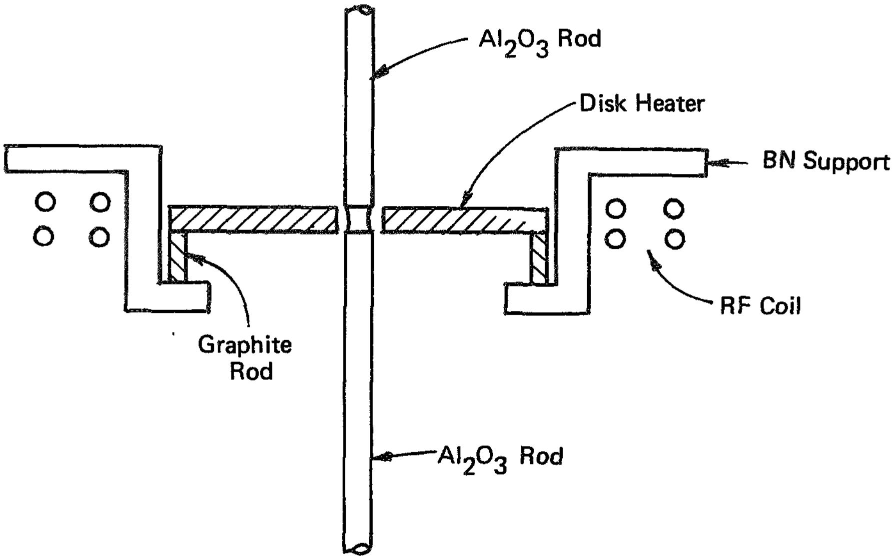

FIGURE 9 IR HEATER USED FOR PRELIMINARY Al_2O_3 GROWTH RUNS

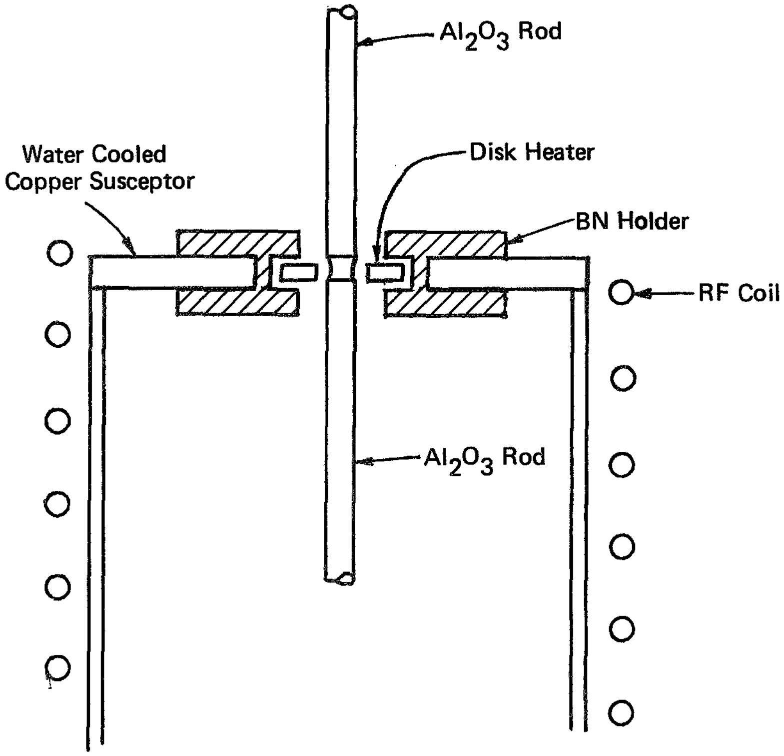

FIGURE 10 MODIFIED IR HEATER USED FOR PRELIMINARY Al_2O_3 GROWTH RUNS

The second coil-heater assembly reduced the electrical potential between the heater and the element which induced current in it (modified concentrator used for direct coupled floating zone crystal growth). The high electrical potential existed between the coil and the concentrator; however, both were cold so the tendency to ionize the gas was reduced. This assembly had substantially better coupling efficiency than the first, and was operated at lower power levels.

2. CO_2 Laser Heat Source

The second fiber growth apparatus designed, built and used during this program used a CO_2 laser as the heat source. The assembled apparatus is shown in operation in Figure 11. The two pulling heads are positioned coaxially in the same positions as they were in the MP Crystal Growing Furnace. The same variable relative shaft speed drive assembly, described above, was used with this apparatus.

The 10 watt Holobeam CO_2 laser shown in Figure 11 was used in all of the laser heated fiber growth experiments. The 0.5 cm diameter laser beam was expanded to approximately 2 cm with the cylindrical beam expander positioned between the laser and the optical bench. This was done to minimize the fraction of the beam energy lost by uncontrolled reflections from the edges of mirror beam dividers.

A schematic representation of the optical bench used in these experiments is shown in Figure 12. Its position just below the plate which supports the upper pulling head is shown in Figure 11. The same bench was used in 1, 2, 3, and 4 beam experiments. In the 4 beam experiments the expanded beam hits plane mirror A and is reflected to plane mirrors B and C positioned such that each mirror receives a half circle of the beam. The semicircular beam from mirror B is interrupted by plane mirrors D and E positioned in the vertical plane such that each receives a quadrant of the beam. A quadrant is reflected from mirror D to the spherical mirror H and the second quadrant from E to the spherical mirror I which focus the beam on the fiber in position L. The beams are depressed 7.5° from the horizontal plane to avoid hitting mirrors D and E. The optical path for the semicircular beam from mirror C is similar. All 7 plane mirrors and 4 spherical mirrors are individually adjustable to provide precise focus-

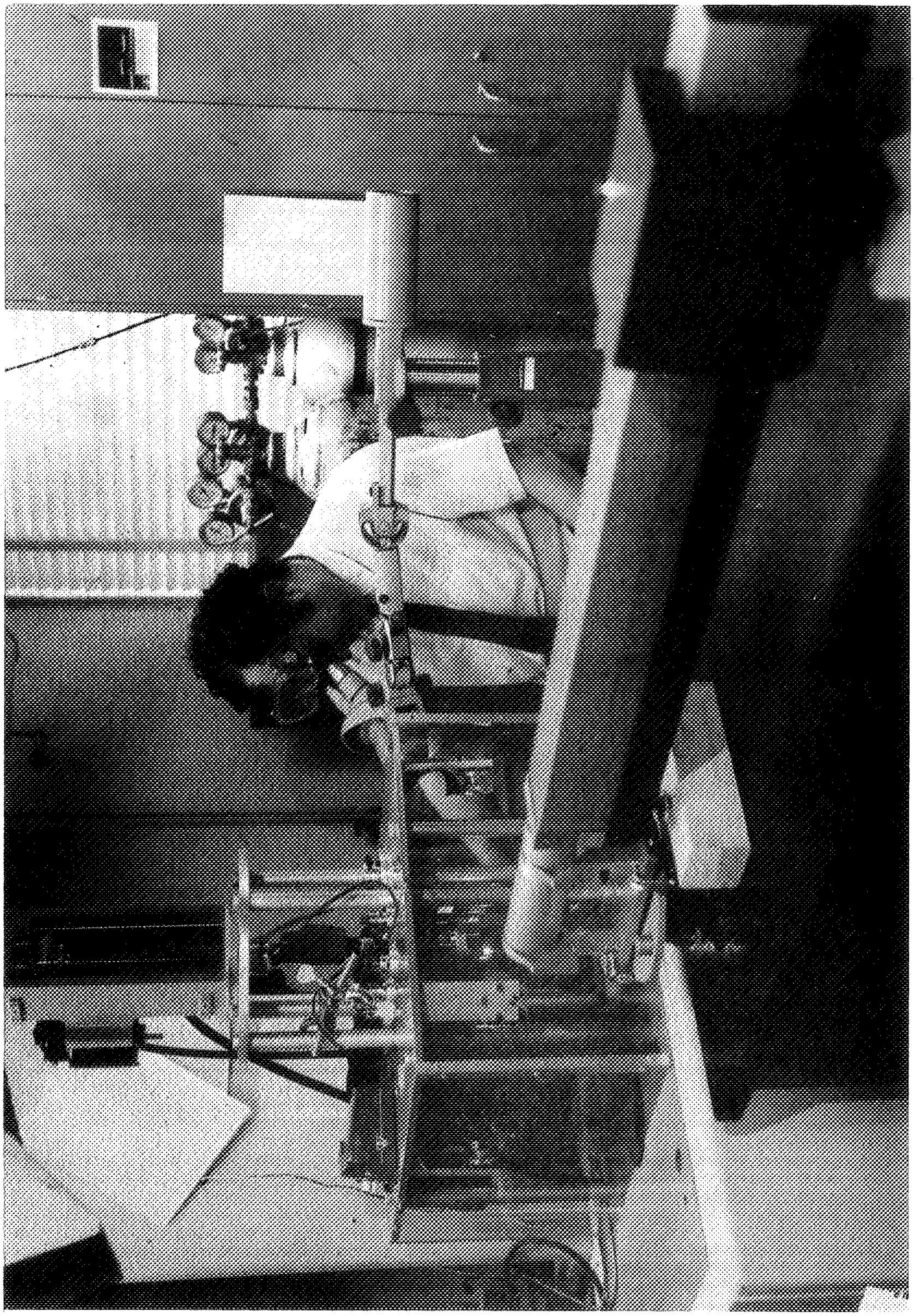

FIGURE 11 CO_2 LASER HEATED FIBER GROWTH APPARATUS

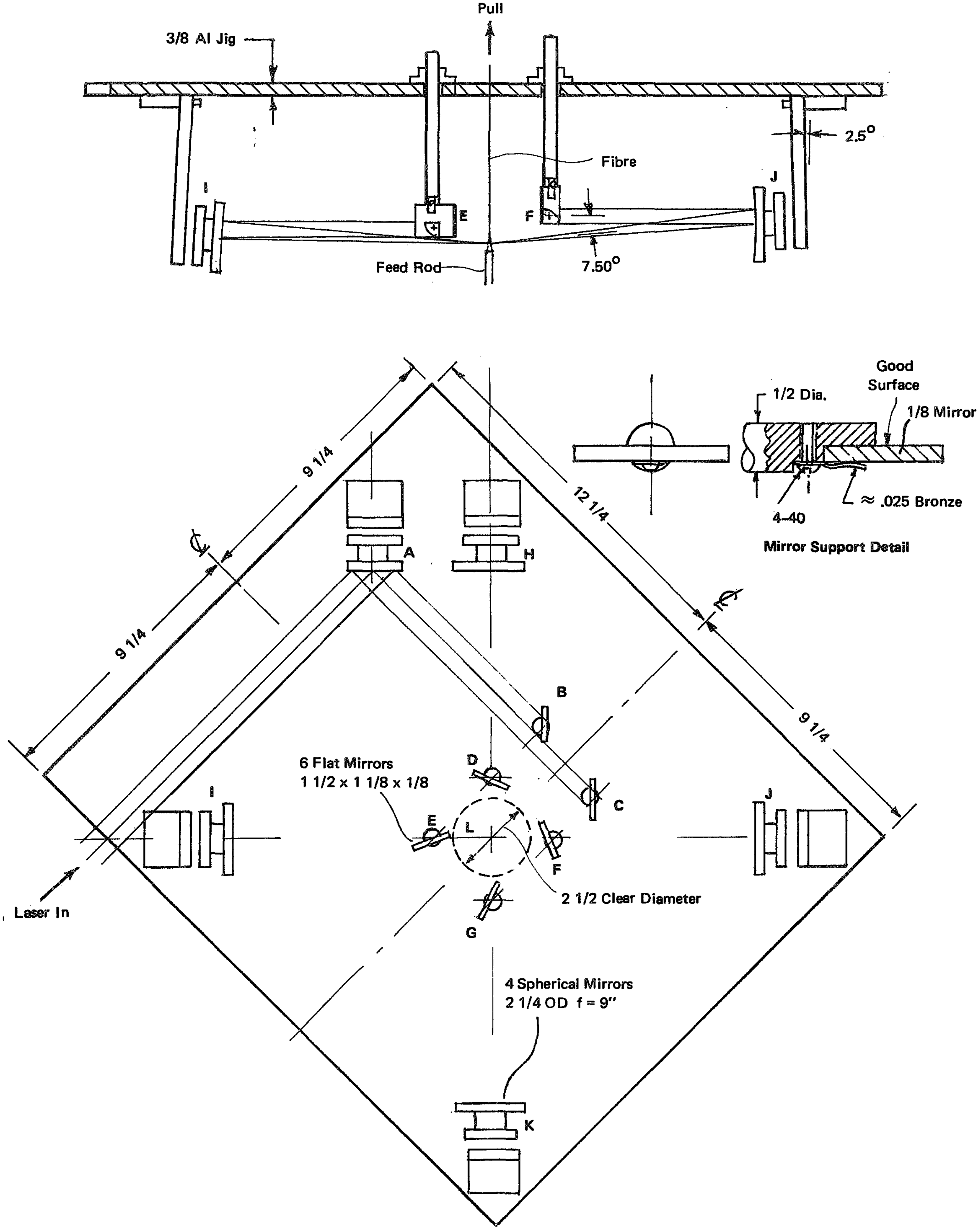

FIGURE 12 SCHEMATIC OF LASER OPTICAL SYSTEM
(DIMENSIONS IN INCHES)

focusing. With this optical system, the beam was focused in spots approximately 0.010 inches (0.0254 cm) in diameter at position L.

In the three beam experiments plane mirror F was removed; in the two beam experiments plane mirrors E and F were removed to reduce the number of times the beam was split. In the one beam experiment plane mirror B was positioned to capture the entire beam.

3. Resistance Heated - IR Source; Fiber Growth Apparatus

The results of preliminary fiber growth experiments carried out in an ADL Model MP Crystal Growing Furnace was encouraging; however, it was evident that the MP furnace system was not well suited to the requirements of this program. Some of the major deficiencies include:

1. inadequate visibility of the fiber-drawing process,
2. Lack of reliable independent control of the fiber-drawing and feed rod insertion rates,
3. lack of horizontal (x-y) adjustment of the fiber and feed rod,
4. insufficiently easy access to the fiber, ceramic-feed rod, heating element and adjacent areas.

Based upon an assessment of the preliminary fiber-drawing experiments, a furnace configuration was developed which overcame these deficiencies. The floating zone fiber-drawing furnace which was constructed is shown schematically in Figure 13 and assembled in Figure 14. Its modular design gives it a high degree of flexibility. The unit can be stretched to permit growth of longer fibers by a batch process, or a take-up reel can be added for semicontinuous operation. Many heating sources, such as rf heated-IR source, CO_2 laser or resistance heated-IR source can be used without modification of the chamber.

The furnace chamber is a rectangular parallel-piped approximately 2 feet (60 cm) high, 1 foot (30 cm) deep and 1 foot (30 cm) wide. Window and access ports were positioned to given maximum flexibility and visibility. During vacuum and 15 psig (2×10^5 N/m^2) operation, stress levels will not

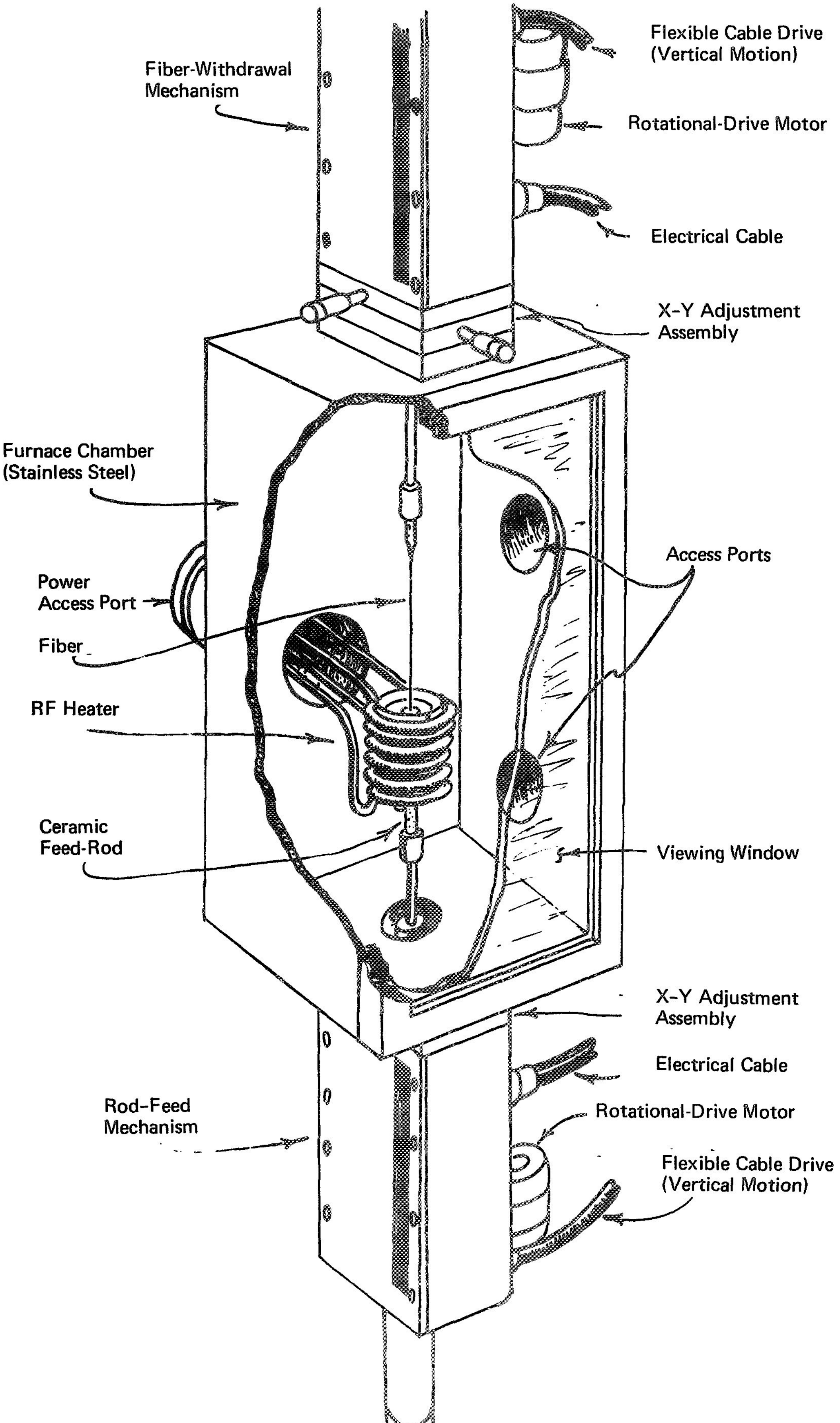

FIGURE 13 SCHEMATIC DRAWING – FLOATING-ZONE FIBER-DRAWING MECHANISM

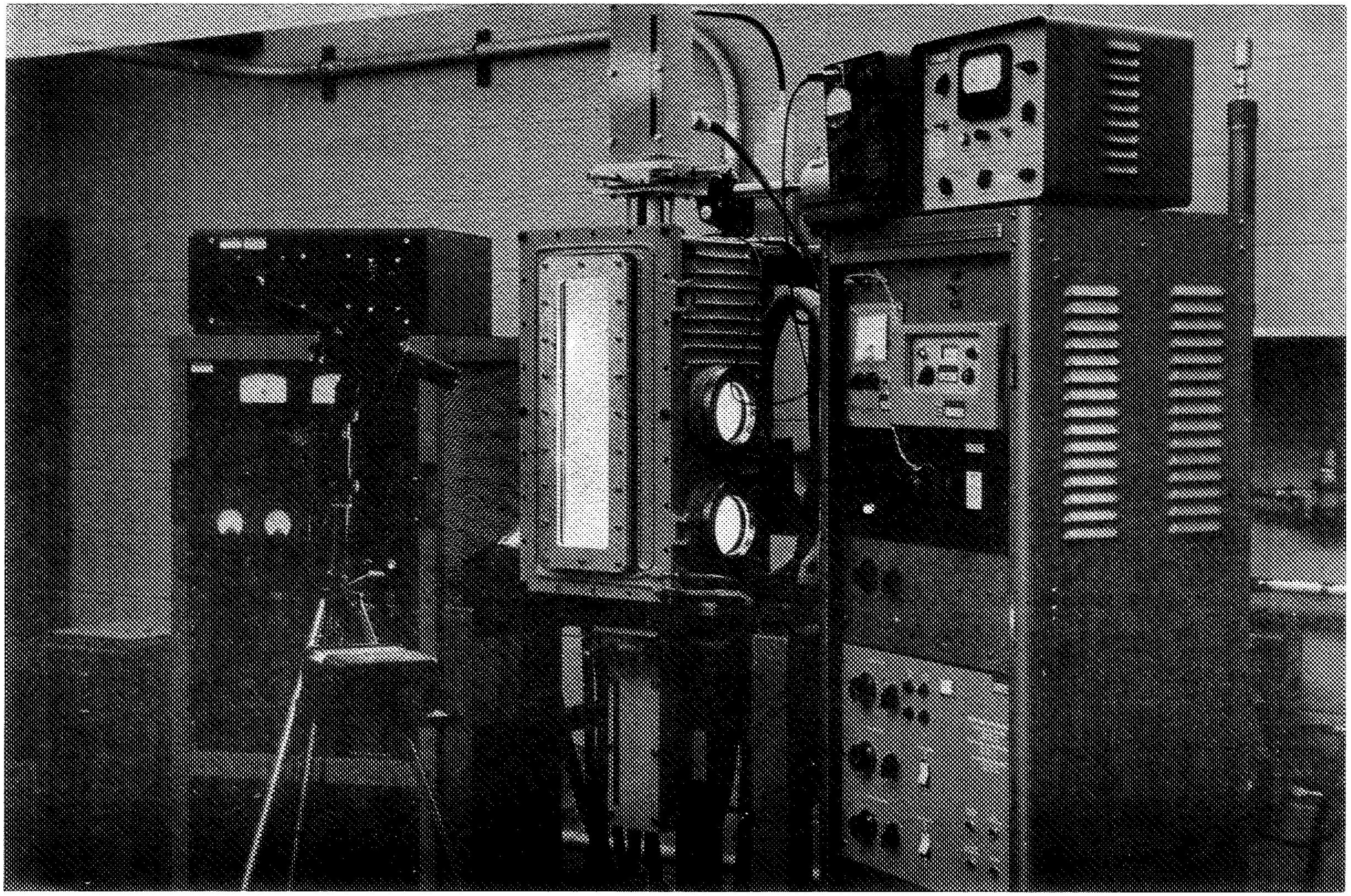

FIGURE 14 PHOTOGRAPH OF FIBER GROWTH APPARATUS 20kw POWER SUPPLY AND CONTROLS

exceed 20,000 psi (1.4×10^8 N/m^2) in the 1/4 inch (0.635 cm) thick water-cooled stainless steel walls and 1000 psi (6.9×10^6 N/m^2) in the 5/8 inch (1.59 cm) thick tempered Pyrex glass window. These stress levels provide adequate margins for safety. The furnace-chamber, pulling-head assembly is supported on rubber shock mounts to minimize vibration transmitted from the support structure. The gear boxes and drive motors for the pulling heads are connected to the furnace by flexible drive cables to minimize the vibration transmitted.

The x-y positioners are based on commercial units manufactured by the Stoelting Company, Chicago, Illinois. It was claimed that dovetails were designed to support both tensile and compressive loading so that the same units were used without modification on upper and lower pulling heads. It has been found that the units have considerable drag when loaded in tension and do not always return under spring loading.

The atmospheric seal in the x-y positioner assembly is provided by a bellows; O-rings form the seal between the bellows and the chamber walls, between the pulling head and the bellows, and between the shaft and the gland assembly.

Fiber withdrawal and feed rod insertion mechanisms are ADL-MP Furnace pulling heads. Unlike the standard MP Crystal Growing Furnace, the rates of travel in these pulling heads can be controlled completely independently.

Where possible, this furnace configuration incorporated standard components and assemblies which have been developed for the ADL Model MP Crystal Furnace to insure reliable operation, the availability of spare parts and to minimize the design and construction costs.

The heating elements were gripped by water-cooled copper connectors. Actual heater element configurations were designed to match the available power supplies and adjusted empirically. The most satisfactory heater configuration found for pyrolytic graphite is shown in Figure 15.

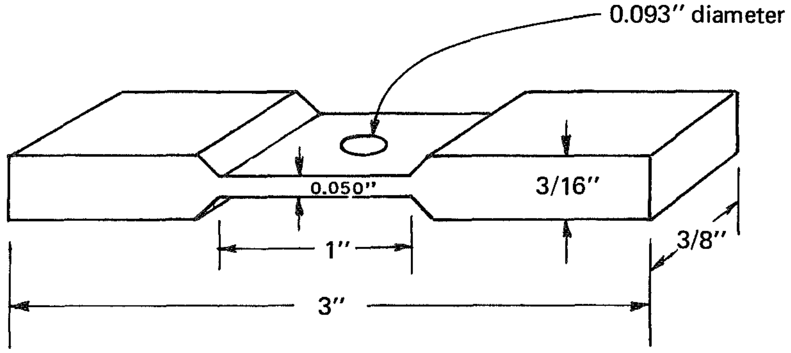

FIGURE 15 PYROLYTIC GRAPHITE HEATER CONFIGURATION SHOWING DIMENSIONS

Flat 1/16 by 1/2 by 3" tungsten heaters were used but unsuccessfully.

Figure 16 is a photograph of a 0.020 inch (0.0508 cm) diameter fiber being grown from a 0.060 inch (0.152 cm) diameter feed rod with an incandescent pyrolytic graphite heater. The water-cooled copper grips are apparent on either side of the heater strip.

Input amperage was monitored by means of a rectified voltage taken from a $50 \times 10^{-3} \Omega$ shunt. This voltage was bucked against a known voltage and their difference used as a control signal for a Leeds & Northrup proportional controller. The amperage was controlled by a saturable core reactor.

Considerable difficulty was experienced in achieving reliable, responsive automatic control of the power level. Proportional controllers must be tuned to the specific characteristics of the heater and feed-back signal. It was found that individual heaters varied to the extent that major adjustments of the controller and power supply were required each time one was changed. The problem was finally resolved by operating the unit with manual control using stabilized voltages for the power supply and control circuitry.

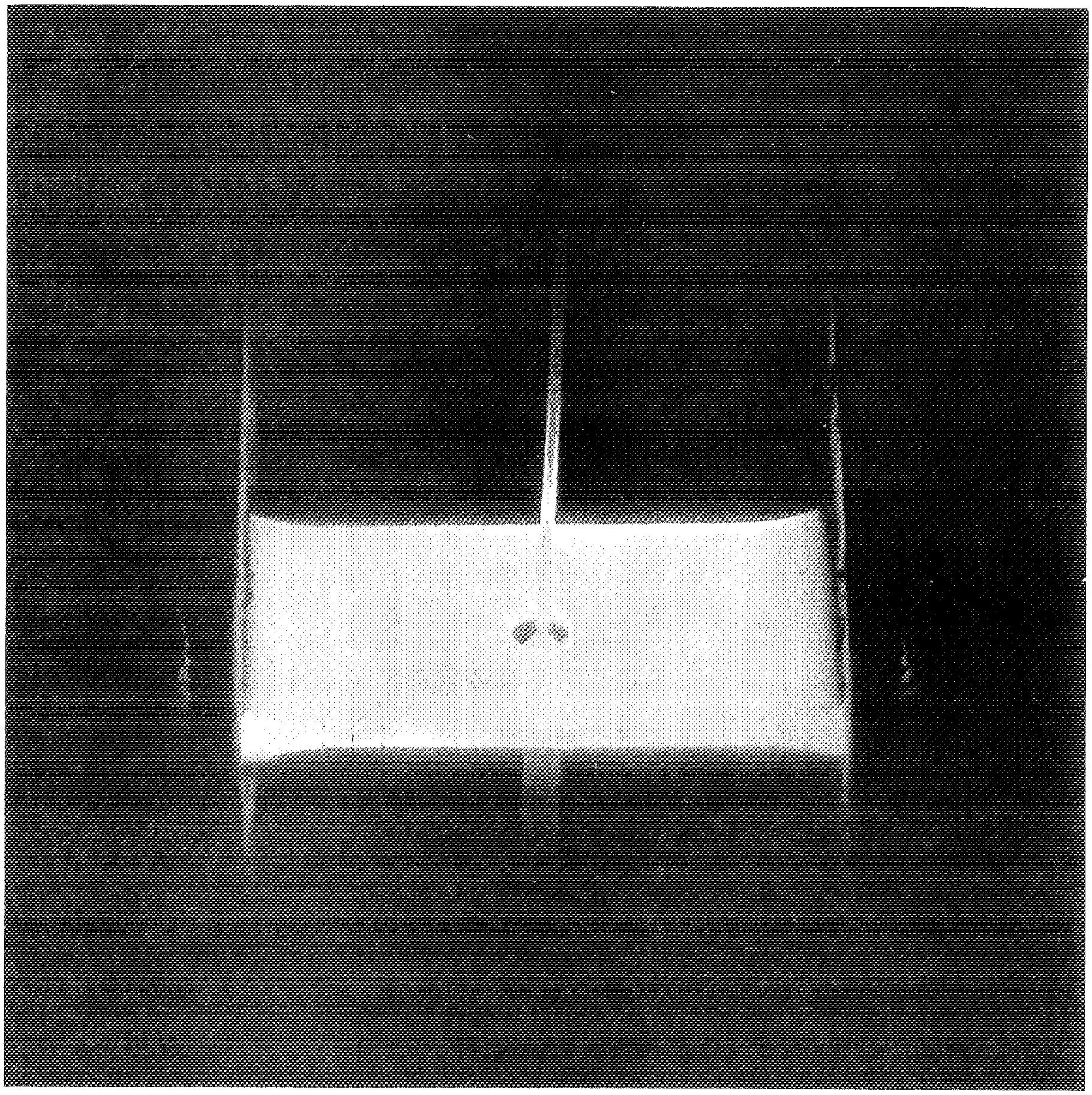

FIGURE 16 PHOTOGRAPH OF FIBER GROWING WITH INCANDESCENT HEATER

IV. SUMMARY OF FIBER GROWTH EXPERIMENTS

The process conditions used for growing the Al_2O_3 fibers produced during this program are summarized in Table III. Heat sources, feed rod materials, feed rod sizes, attenuation ratios, growth rates, direction of growth and ambient atmospheres were the process parameters examined. Specific process conditions investigated were:

A. Feed Rod Materials

1. McDanel AP-35
2. McDanel AV-30
3. Coors 995 (pink)
4. Linde Single Crystal Ruby
5. Degussa AL-23

Diameters of feed rods ranged from 0.016 to 0.125 inches (0.0406 to 0.318 cm). Chemical analyses of the feed rods are summarized in Table IV.

TABLE IV

SUMMARY OF FEED ROD CHEMICAL ANALYSES

(percentage by weight)

Impurity	McDanel AP-35	McDanel AV-30	Coors 995 (pink)	Linde Ruby	Degussa AL-23
Cr_2O_3			.22	5.8	
SiO_2	.7	3.0	.16	.13	.1
Fe_2O_3	.07	.1	.05	.29	.05
MnO				.013	
MgO	.07	1.1	.23	.05	.2
SnO_2				.057	
CaO	.03	.22	.05		.05
Na_2O	.05	.06	.05		.2
B_2O_3			.07		

B. Heating Technique

1. Incandescent Heater

a.	pyrolytic graphite	(Raytheon, Union Carbide)
b.	graphite	(Ultra Carbon)
c.	vitreous carbon	(Atomergic Chemetals)
d.	tungsten	(General Electric)
e.	molybdenum	(unknown source)

2. CO_2 Laser

a. a 10 watt Holobeam model 20-1

C. Growth Conditions

1. up and down pulling
2. seeded and unseeded growth
3. attenuation ratios between 1/1 to 20/1 (length basis)
4. growth rates between 0.7 to 70 inches (1.7 to 170 cm) per hour
5. air, argon, helium, nitrogen, nitrogen-hydrogen, argon-helium, and vacuum atmospheres.

TABLE III

SUMMARY OF FIBER GROWTH RUNS

Run No.	Heating Assembly	Heater Material	Heater Thickness (in.)	Hole Size (in.)	Feed Rod Material	Feed Rod Diameter (in.)	Atmosphere (psig)	Zone Temperature (°F)	Cavity Temperature (°F)	Top of Heater Temperature (°F)	Growth Rate (in/hr)	Attenuation Ratio Growth Rate / Feed Rate	Comments
1	I	graphite	0.250	0.250	A	0.125	10(N_2)	3416	3704	---	2.0	----	Al_2O_3 melted and filled carbon cavity, dark coloration observed.
2	I	graphite	0.125	0.250	A	0.125	10(N_2)	3380	3812	---	2.0	----	Al_2O_3 melted, dark coloration.
3	I	graphite	0.125	0.250	B	0.125	10(N_2)	3452	3992	---	2.0	----	Al_2O_3 had an outer core of dark material and an inner core of what appears to be unmolten material.
4	I	graphite	0.125	0.1875	A	0.125	10 (90%N_2-10%H_2)	----	----	---	2.0	----	Material did not melt, but evidence of appreciable deposits of carbon on the alumina feed rods.
5A	I	graphite	0.1875	0.250	A	0.125	10(Ar)	3218	3668	---	2.0	----	Severe arcing.
5B	I	graphite	0.1875	0.250	A	0.125	30(Ar)	3218	3704	---	2.0	----	Arcing.
5C	I	graphite	0.1875	0.250	A	0.125	15(30%Ar-70%He)	3488	4028	---	2.0	----	Could just melt lower rod, system appeared cleaner.
6	I	graphite	0.1875	0.250	A	0.125	10(N_2)	3344	3920	---	2.0	----	Al_2O_3 melted, but dark coloration.
7	I	graphite	0.1875	0.250	A	0.125	10^{-4} torr	3434	3812	---	2.0	----	Melting and some necking of sample when lower rod was fed in at a slower rate than top rod. However, sample appeared milky. Arcing also appeared which caused a shut-down of the system.
8	II	graphite	0.062	0.1875	A	0.125	10(Ar)	3488	4262	4262	2.0	----	Partial melting, but carbon disk developed a crack.
9	II	graphite	0.125	0.1875	A	0.125	10(Ar)	3416	4028	4028	2.0	----	Material melted rapidly. Lost zone.
10	II	graphite	0.125	0.1875	A	0.125	10(Ar)	----	----	---	2.0	1:1 to 3:1	Material melted and necked down by controlling lower rod feed rate.
11	II	Mo	0.062	0.1875	A	0.125	10(Ar)	----	3524	---	2.0	----	Molybdenum melted (possible reaction with BN)
12	II	W	0.130	0.1875	A	0.125	10(Ar)	3416	3956	---	2.0	----	Tungsten showed molten surface (reaction with BN)
13	II	P.G.	0.125	0.250	A	0.125	10(Ar)	3452	4352	3488	2.0	1:1 to 6:1	3.5 inches of fiber grown with attenuation ratio changed in steps until lost zone at 7:1.
14	II	P.G.	0.125	0.250	B	0.125	10(Ar)	3272	4424	4028	2.0	----	Difficult to see melting, lost zone.
15	II	P.G.	0.125	0.250	B	0.125	10(Ar)	3713	4622	4136	2.0	----	Initially necked down Al_2O_3 but the rod solidified and when remelted the zone was lost.
16	II	P.G.	0.125	0.156	C	0.125	10(Ar)	----	4352 +	3714 +	2.0	----	Easy start, but lot of vaporization and whisker formation, probable contact with heater--lost zone.
17A	II	P.G.	0.125	0.1875	C	0.125	10(Ar)	3344	4208 +	3416 +	2.0	----	Started zone, but touched heater, zone lost--temperature measured prior to initiation of growth.
17B	II	P.G.	0.125	0.1875	C	0.125	10(Ar)	3344	4208	3416	2.0	1:1 to 10:1	Grew 4 inches of fiber while progressively changing attenuation to 10:1, then saw zone shape change and lost zone at 11:1. Temperature measured prior to initiation of growth.
18A	II	P.G.	0.125	0.1875		----	10(Ar)	----	3884	3056	--	----	Raytheon P.G. no change noticed after heating 10 minutes.
18B	II	P.G.	0.125	0.1875		----	10(Ar)	----	4280	3326	--	----	Raytheon P.G. heated 10 minutes, slight change in coloration where BN was in contact with P.G.
18C	II	P.G.	0.125	0.1875		----	10(Ar)	----	4694	3722	--	----	Temperature drop of 160° F in 10 minutes, carbon ring 0.003 inches thick on outside diameter of P.G.

TABLE III (Cont.)

SUMMARY OF FIBER GROWTH RUNS

Run No.	Heating Assembly	Heater Material	Heater Thickness (in.)	Hole Size (in.)	Feed Rod Material	Feed Rod Diameter (in.)	Atmosphere (psig)	Zone Temperature (°F)	Cavity Temperature (°F)	Top of Heater Temperature (°F)	Growth Rate (in./hr)	Attenuation Ratio $\frac{\text{Growth Rate}}{\text{Feed Rate}}$	Comments
18D	II	P.G.	0.125	0.1875	-	----	10(Ar)	----	5072	4028	--	----	Temperature drop of 500° F in 10 minutes, some delamination evident.
18E	II	P.G.	0.125	0.1875		----	10(Ar)	----	5198	4316	--	----	Temperature drop of 500° F in 10 minutes, delamination evident.
19A	II	P.G.	0.125	0.1875		----	10(Ar)	----	4307	3452	--	----	Union Carbide Pyrolytic graphite. No change after 10 minutes heating.
19B	II	P.G.	0.125	0.1875	-	----	10(Ar)	----	4667	3740	--	----	Temperature drop of 80° F after 10 minutes.
19C	II	P.G.	0.125	0.1875	-	----	10(Ar)	----	4892	4064	--	----	Temperature drop of 320° F after 10 minutes--see delamination taking place.
20A	II	graphite	0.125	0.1875		----	10(Ar)	----	3992	----	--	----	Graphite needed more power from RF unit to reach this temperature--slight reaction.
20B	II	graphite	0.125	0.1875		----	10(Ar)	----	4352	----	--	----	Temperature drop of 90° F in 10 minutes--reaction with boron nitride.
21	II	P.G.	0.125	0.1875	C	0.125	10(Ar)	----	----	----	2.0	1:1 to 10:1	2.5 inches of fiber grown at varying attenuation ratios up to 10:1--1.5 inches of 10:1 attenuation ratio grown at 2 inches/hour, but zone diameter not stable--on increase of pulling speed material necked off.
22	II	P.G.	0.125	0.1875	C	0.125	10(Ar)	3920	4388	3560	2.0	1:1 to 9:1	5 inches of fiber grown; when molten zone is below P.G. cone shape flattens out and fibers separate after a while, when molten zone is kept inside P.G. heated zone (i.e., less power). A stable growth zone was maintained at an attenuation ratio of 9:1.
23	II	P.G.	0.125	0.1875	D	0.125	10(Ar)	3398 +	4352 +	3542+	7.0	10:1	3.5 inches of fiber grown without interruption at a constant attenuation ratio; molten zone visible in heater. Temperature measured prior to initiation of growth.
24	II	P.G.	0.125	0.1875	D	0.125	10(Ar)	----	----	----	7.0	20:1	0.25 inches of fiber grown; could not maintain zone.
25	II	P.G.	0.125	0.1875	D	0.125	10(Ar)	----	----	----	--	----	Pyrolytic graphite hole was tapered at 45° for 0.062 inches at the base. Could not see molten zone.
26	II	P.G.	0.125	0.1875	D	0.125	10(Ar)	3416	4172 +	3272+	21	10:1	2.5 inches of fiber grown without interruption at a constant attenuation ratio after several starts. Total fiber length exceeds 5 inches. Temperature measured prior to initiation of growth.

TABLE III (Cont.)

SUMMARY OF FIBER GROWTH RUNS

Run No.	Heating Assembly	Heater Material	Heater Thickness (in.)	Hole Size (in.)	Feed Rod Material	Feed Rod Diameter (in.)	Atmosphere (psig)	Zone Temperature (°F)	Cavity Temperature (°F)	Top of Heater Temperature (°F)	Growth Rate (in./hr)	Attenuation Ratio Growth Rate / Feed Rate	Comments
27	II	P.G.	0.125	0.1875	D	0.125	10(Ar)	----	----	----	--	10:1	Could not start a run at speeds faster than 21 inches per hour.
28	II	P.G.	0.125	0.1875	D	0.125	10(Ar)	----	----	----	7	2:1	Pyrolytic graphite hole was tapered at 45° for 0.062 inches at the top. Could not maintain molten zone.
29	II	Vitreous Carbon	0.081	0.216	D	0.125	10(Ar)	3308+	4064+	----	--	----	Vitreous carbon cracked right after Al_2O_3 melted--try smaller hole size.
30	II	P.G.	0.063	0.1875	D	0.125	10(Ar)	3704	4496	3992	3-70	2:1-10:1	With an attenuation ratio of 10:1 could not go over 20 inches per hour; with an attenuation ratio of 3:1 went as high as 70 inches per hour but obtained a very nonuniform rod diameter.
31	II	Vitreous Carbon	0.081	0.185	D	0.125	10(Ar)	----	----	----	--	----	Got to melting point of Al_2O_3, but carbon cracked.
32	II	P.G.	0.063	0.125	D	0.063	10(Ar)	3722	4496	4118	2	10:1	Zone unstable--had several starts but only obtained 1/2 inch of material.
33	II	P.G.	0.125	0.125	D	0.063	10(Ar)	----	----	----	--	----	Zone molten but visibility too limited for fiber attenuation.
34	II	P.G.	0.063	0.0937	D	0.063	10(Ar)	3776	4442	3902	7	10:1	Got 5-1/2 inches Al_2O_3 fiber with one restart.
35	II	P.G.	0.063	0.0937	D	0.063	10(Ar)	3848	4496	3992	21.5	10:1	Got 7 inches Al_2O_3 fiber.
36	II	P.G.	0.063	0.0937	D	0.063	10(Ar)	----	----	----	7-60	10:1	Could grow at speeds up to 60 inches per hour--separated at 70 inches per hour.
37	II	P.G.	0.063	0.0937	D	0.063	10(He)	3668	4316	3632	13	10:1	Grew 6 inches of fiber--rough surface.
38	II	P.G.	0.063	0.0937	D	0.063	10(He)	----	----	----	10-20	10:1	Grew 6 inches of fiber at different pulling speeds--rough surface.
39	II	P.G.	0.063	0.0937	D	0.063	-11(Ar)	----	----	----	13	5:1	Could not grow with attenuation ratios greater than 5:1.
40	II	P.G.	0.063	0.0937	D	0.063	-11(Ar)	3884	4442	3812	2	5:1	Could not grow with attenuation ratios greater than 5:1.
41	II	P.G.	0.063	0.0937	D	0.063	10(He)	----	----	----	2	10:1	Surface rough.

TABLE III (Cont.)

SUMMARY OF FIBER GROWTH RUNS

Run No.	Heating Assembly	Heater Material	Heater Thickness (in)	Hole Size (in)	Feed Rod Material	Feed Rod Diameter (in)	Atmosphere (psig)	Zone Temperature (°F)	Cavity Temperature (°F)	Top of Heater Temperature (°F)	Growth Rate (in/hr)	Attenuation Ratio Growth Rate / Feed Rate	Comments
42A	III				C	.063	Air						Could not melt completely. Noticed 4 molten craters. Spot size estimated at 0.010".
42B	III				C	.032	Air						Could not melt.
42C	III				E_1	0.020	Air				2-7	2:1-7:1	Melted easily. Grew 5". Surface quite rough.
43	III				E	0.020	Air				2	3:1-6:1	Four inches of fiber grown. Surface much smoother than 42C. Golden color appearance to fiber.
44	III				E	0.020	Air				2	3:1	Five inches of fiber grown.
45	III				E	0.020	Air				1.3-7	4:1	Seven and one-half inches of fiber grown. Fluctuation in diameter probably due to non-uniform feed rate.
46	III				E	0.020	Air				7	4:1	Seven and one-half inches of fiber grown.
47	III				E	0.020	Air				3.4*	1:1	Three and one-half inches of fiber grown. The fiber was grown in a downward direction.
48	III				E	0.016	Air				0.7-2	1:1-3:1	Zone unstable and difficult to control. Long zone obtained due to too much power
49	III				E	0.016	Air				0.7-2	3:1-4:1	Lazer power decreased with variable transformer. Six inches of fiber grown.
50	III-A				E	0.020	Air				2	4:1	Rod heated from three sides (2-180° apart 3rd 90° from other two). Grew 5" of material with an off center zone.
51	III-B				E	0.020	Air				2	4.5:1	Three and one-half inches of fiber grown. Zone more difficult to maintain.
52	III-C				E	0.020	Air				2	4.5:1	Three and one-half inches of fiber grown. Zone difficult to maintain. Growth zone off center and separated easily.
53	III				E	0.020	Air				2.0-7.1	5.5:1	Seven inches of 0.0085" diameter fiber growth. Zone appeared more stable at highest growth rates.
54	III				E	0.020	Air				2.0	5.5:1	Four and one-half inches of 0.008" diameter fiber grown.
55	III				E	0.020	Air				2.0	5.5:1	Eight inches of 0.008" diameter fiber grown.
56	III				E	0.020	Air				2.0-7.1	5.5:1	Seven inches of 0.008" diameter fiber grown.

* down-pull

TABLE III (Cont.)

SUMMARY OF FIBER GROWTH RUNS

Run No.	Heating Assembly	Heater Material	Heater Thickness (in.)	Hole Size (in.)	Feed Rod Material	Feed Rod Diameter (in.)	Atmosphere (psig)	Zone Temperature (°F)	Cavity Temperature (°F)	Top of Heater Temperature (°F)	Growth Rate (in/hr)	Attenuation Ratio $\frac{\text{Growth Rate}}{\text{Feed Rate}}$	Comments
57	III				E	0.020	Air				1.3-7.1	4:1	Four inches of 0.010" diameter fiber grown. Smoother fiber at highest growth rates.
58	III				E	0.016	Air				1.0	1:1	Difficulty maintaining zone. Rough fiber produced.
59	III				E	0.020	Air				2.0-7.1	5.5:1	Smooth fiber grown. Alignment reasonably good.
60	III				E	0.020	Air				5.2	5.5:1	Same observation as Run 59.
A-1	IV	P.G.	0.050	0.093	E	0.062	-5(Ar)		4565	4280	4.35 *	3.6	Fiber pulled in downward direction. Bubbles observed bursting on surface of zone. Rough fiber.
A-2	IV	P.G.	0.050	0.093	E	0.062	1(Ar)		4585+	4135-4460	3-8.7	1:1-4.8:1	Heater burned out during run.
A-3	IV	P.G.	0.050	0.080	E	0.062	1(Ar)		4585	3955-4010	1.2-8.7	1:1-7.3:1	Saturable core reactor power supply run on manual control. Fiber diameter fluctuated when freezing interface approximately 0.020 above surface of heater. Smooth fiber when located at upper surface of heater.
A-4	IV	P.G.	0.050	0.080	E	0.062	1(Ar)			3990-4100	8.7:17.4	7.2	Four inches of 0.020" diam. fiber grown at 8.7"/hr and remainder at 17.4"/hr. Freezing interface moved up above heater at higher growth rate. Heater temperature lower to bring freezing interface to same level as top heater.
A-5	IV	P.G.	0.050	0.080	E	0.062	1(Ar)			4065	17.4	7.4	Feed rod zone melted at 23.8"/hr and 1:1 attenuation ratio in downward direction then fiber grown in upward direction from premelted feed rod.

* down-pull

TABLE III (Cont.)

SUMMARY OF FIBER GROWTH RUNS

Run No.	Heating Assembly	Heater Material	Heater Thickness (in.)	Hole Size (in.)	Feed Rod Material	Feed Rod Diameter (in.)	Atmosphere (psig)	Zone Temperature (°F)	Cavity Temperature (°F)	Top of Heater Temperature (°F)	Growth Rate (in/hr)	Attenuation Ratio Growth Rate / Feed Rate	Comments
Batch 1	IV	P.G.	0.050	0.093	D	0.063	1(Ar)		4460-4660	3955-4280	22.8	10/1	Ten unseeded fibers grown. Control of process good.
Batch 2	IV	P.G.	0.050	0.093	D	0.063	1(Ar)			4030-4250	22.8	10/1	Ten fibers grown using 0° TYCO fiber as seed. Control of process good.
Batch 3	IV	P.G.	0.050	0.093	D	0.063	1(Ar)			4170-4210	43.5	10/1	Five fibers grown. Fiber diameter oscillated. Fiber vibration noted.
Batch 4	IV	P.G.	0.060	0.093	D	0.063	1(Ar)			4040-4150	22.8	10/1	Eight fibers grown. Fiber diameter tended to oscillate and control more difficult than Batches 1 and 2.
Batch 5	IV	P.G.	0.060	0.093	F	0.063	1(Ar)			3940-4030	22.8	10/1	Five fibers grown. Control better than in Batch 4.
Batch 6	IV	P.G.	0.060	0.093	D	0.063	1(Ar)			4030-4065	22.8*	10/1	Eleven fibers grown in downward direction. Control of process good after third fiber. Zone appeared to have different shape than up-pull.
Batch 7	IV	P.G.	0.063	0.093	D	0.063	1(Ar)			3830-4030	22.8	10/1	Six fibers grown from feed rod which was premelted in vacuum. Fiber 7-E grown in vacuum. Fiber diameter tended to oscillate.
Batch 8	IV	P.G.	0.050	0.093	C	0.062	1(Ar)			3900-4000	22.8	10/1	Zone difficult to maintain. Fibers had rough, porous texture.
Batch 9	IV	P.G.	0.050	0.093	D	0.062	1(Ar)		4800	4320	22.8	10/1	Zone difficult to maintain. Zone broke off as if too cold when temperature lowered to point where diameter did not oscillate.
Batch 10	IV	P.G.	0.050	0.093	G	0.062	1(Ar)			4500	22.8	10/1	Heater filament failed when reached sufficiently high temperature to melt single crystal feed rod. Could not sustain fiber growth run.
Batch 11	IV	P.G.	0.050	0.093	D	0.062	1(He)			3100	22.8	10/1	Bursting bubbles on zone adjacent to fiber made it difficult to maintain stable zone. Rough surface on fiber.
Batch 12	IV	P.G.	0.050	0.093	D	0.062	1(He)			3900	22.8*	10/1	Bursting bubbles caused zone to neck off every 1/2 inch of growth.
Batch 13	IV	P.G.	0.050	0.093	D	0.062	1(He)	3630	4300	3940	2.17	10/1	Bursting bubbles caused zone and fiber to vibrate. Rough surface on fiber.
Batch 14	IV	P.G.	0.050	0.093	D	0.062	1(Ar)			4030-4100	22.8*	10/1	Reproducing Batch 6 for high temperature tensile samples.
Batch 15	IV	P.G.	0.050	0.093	F	0.062	1(Ar)			4030-4170	22.8*	10/1	Reproducing Batch 5 for high temperature tensile samples.
Batch 16	IV	P.G.	0.050	0.093	D	0.062	1(Ar)			4060-4140	22.8*	10/1	Reproducing Batch 6 for high temperature tensile samples.
Batch 17	IV	P.G.	0.050	0.093	F	0.062	1(Ar)			4080	22.8*	10/1	Reproducing Batch 5 for high temperature tensile samples.

*downpull

Notes

I = rf coil, BN support, disk heater
II = rt coil and concentrator
III = 10 watt laser assembly heating from 4 sides
IIIA = 10 watt laser assembly heating from 3 sides
IIIB = 10 watt laser assembly heating from 2 sides
IIIC = 10 watt laser assembly heating from 1 side
IV = resistance heated
A = McDanel AP 35, 4 hole Al_2O_3 insulating tube
B = Sapphire single crystal
C = McDanel AV 30 solid rod
D = McDanel AP 35 solid rod
E = Degussa AL-23
E1= Degussa AL-23 hollow tube
F = Coors AD 995 (pink)
G = Linde Single Crystal Ruby

V. RESULTS AND DISCUSSION OF FIBER GROWTH AND EVALUATION PROGRAM

A. Thermal Analysis

The agreement between predicted incandescent filament temperatures and the actual "cavity" temperatures required to produce stable, molten zones of Al_2O_3 was generally good despite the unrealistic approximations that were made for zone shape. Predicted temperatures were 4350, 4685, and 4930°F (2400, 2585, and 2720°C) respectively for zero, 1/2 feed rod radius and 1 feed rod radius clearance between the feed rod and graphite heater. With few exceptions, operative temperatures ranged between 4350 and 4500°F (2400 and 2485°C) in the cavities of pyrolytic graphite and graphite heaters. There was sufficient variation between operating temperatures observed with different heaters under nominally identical growth conditions that there is little use in making a detailed examination of the effect of varied geometry and ambient atmosphere on operating temperature. It can be said that the observed temperatures were generally lower than calculated temperatures. This discrepancy can be attributed in part to sighting on the filament through a 1/2 inch (1.27 cm) thick Pyrex window by way of a mirror inside the furnace. Observations made directly on the filament were approximately 150°F (85°C) hotter than when the mirror was used. The latter was generally done to provide a better viewing angle. Also, calibration of the pyrometer to NBS standards indicated that indicated temperature (Micro Optical Pyrometer, Pyrometer Instrument Co., Bergenfield, Vermont) were low by approximately 135°F (75°C) in this temperature range. The values reported in Table III are uncorrected readings. With these two corrections, the operating temperatures are more nearly in agreement with those calculated for graphite heaters and polycrystalline feed rods.

Single crystal sapphire and ruby feed rods were not successfully melted in fiber growth runs. The surfaces of these feed rods appeared molten (Runs 2, 14, 15 and Batch 10); however, the zones behaved as if they were not molten across their entire cross sections. It is probable that the absence of photon scattering in these pore-free, single crystal feed rods did in fact result in incomplete melting of the feed rod. At these temperatures, the fraction of heat transmitted by photons can exceed that transmitted by phonons by several orders of magnitude when scattering sites are eliminated.(2) Pyrolytic graphite heaters degraded and failed when cavity temperatures exceeded 4700°F (2600°C).

All attempts to use tungsten and molybdenum incandescent heaters were unsuccessful. In the rf heated apparatus used in the initial runs, the metals reacted with BN insulators at temperatures that were well below those required for fiber growth. The 0.062 inch (0.151 cm) diameter Al_2O_3 feed rods were melted with 0.060 inch (0.152 cm) thick tungsten heaters with 0.080 inch (0.203 cm) diameter holes at indicated temperatures of approximately 4170°F (2300°C). Again, this compares favorably with 5075°F (2800°C) calculated for a closely coupled feed rod and incandescent heater when the same temperature corrections plus that attributed to the low emissivity are made. Fibers could not be drawn from these molten zones because the melts became contaminated when the feed rods contacted the heaters. Distortions, which occur during heating, exceeded the clearance between the heater and feed rods in these runs.

The results of the power requirement analysis for CO_2 laser heat sources are summarized in Table V. These results were based on the same assumed geometry used for incandescent filament heaters and were found to be in good agreement with reported laser melting experiments when scaled down to the correct dimensions.(3,4)

TABLE V

ESTIMATED POWER REQUIREMENTS FOR CO_2 LASER HEATING

	Molten Zone Height		Molten Zone Diameter		Radiation Loss	Conduction Loss	Total
	(in)	(cm)	(in)	(cm)	(watts)	(watts)	(watts)
Unshielded	0.1	0.254	0.1	0.254	32	13	45
	0.05	0.127	0.05	0.127	5.5	4.4	9.9
	0.05	0.127	0.1	0.254	19	13	32
	0.025	0.063	0.05	0.127	3.3	4.4	7.7
One Shield around Molten Zone	0.1	0.254	0.1	0.254	15	13	28
	0.05	0.127	0.05	0.127	2.6	4.4	7.0

These estimates assumed that the pulled fiber is small compared to the feed rod. While not accounting for the shape of the zone in detail, these estimates suggested that a 10 watt unit would be capable of melting a feed rod 0.05 inch (0.127 cm) in diameter, unshielded and a slightly larger rod if it were shielded.

On the basis of these calculations, the 10 watt CO_2 laser and optical bench described in a previous section was assembled. The optics were designed to focus the beam into four 0.010 inch (0.0254 cm) diameter spots on the feed rod.

Initial attempts to melt 0.031 inch (0.0787 cm) and 0.062 inch (0.157 cm) diameter feed rods were unsuccessful. Four molten craters were produced on the larger feed rod and the entire cross section of the 0.031 inch (0.0787 cm) diameter feed rod could not be melted. Feed rods 0.020 inch (0.05 cm) in diameter were easily melted and fibers drawn from them. The zones produced with 0.016 inch (0.0406 cm) diameter feed rods with full laser power were too long to be stable.

The output power of the laser was not measured calorometrically, so it is not possible to comment with certainty whether the apparent discrepancy in melting capacity resulted from inaccurate calculations, lower than rated output power from the laser, or losses in the mirror optics.

It is clear that the analyses were quite accurate despite the unrealistic zone shape that was assumed. It is probable that it would be useful to expand the analyses to include the effect of small levels of porosity on heat transferred through the fiber because radiant (photon) heat transfer can exceed phonon transfer by several orders of magnitude in Al_2O_3 when it is free of scattering sites. If incandescent heater fiber growth experiments were to be continued, it would be advisable to consider the zone shape - heat transfer problem in detail to analyze the effect of variable heat-transfer coupling-efficiency on zone stability.

B. Fiber Morphology and Microstructural Features

1. Shape and Dimensional Uniformity

The fibers had excellent axial and radial dimensional uniformity when produced under growth conditions where regular, cyclic diameter fluctuations did not persist. The results of micrometer measurements of eight representative fibers are given in Table VI.

TABLE VI

FIBER DIMENSIONS

Fiber	Nominal Diameter (in)	Nominal Diameter (cm)	Average Diameter (in)	Average Diameter (cm)	Standard Deviation (in)	Standard Deviation (cm)	Number of Measurements	Equivalent Diameter(in) from wt/length (in)	Equivalent Diameter(in) from wt/length (cm)	Difference (percent)
23	0.040	0.102	0.0404	0.1026	0.00050	0.00127	18			
16-C	0.020	0.0508	0.0206	0.0523	0.00049	0.00124	10	0.0193	0.0490	6.3
16-F	0.020	0.0508	0.0200	0.0508	0.00029	0.000737	10	0.0197	0.0500	1.5
16-G	0.020	0.0508	0.0196	0.0498	0.00052	0.00132	10	0.0192	0.0488	2.0
16-E	0.020	0.0508	0.0205	0.0521	0.00028	0.000711	10	0.0196	0.0498	4.3
17-A	0.020	0.0508	0.0194	0.0493	0.00056	0.00142	10	0.0190	0.0483	2.0
17-B	0.020	0.0508	0.0194	0.0493	0.00035	0.000889	10	0.0190	0.0483	2.0
17-D	0.020	0.0508	0.0198	0.0503	0.00035	0.000889	10	0.0193	0.0490	2.5

When fibers were grown under conditions where the incandescent filament thickness exceeded the fiber diameter by more than 2.5 times and/or if the incandescent heater was too hot, the diameter of the fiber cycled about its mean value. The wavelengths of the fluctuations were in reasonable agreement with the values predicted by Equation 10 (5 to 10 fiber diameters); however, the amplitude did not diminish as predicted. The persistence of the oscillation is believed to result from interaction of heat transmitted to the zone and zone shape. It is suspected that the assumption of constant zone height was not realized with the closely-coupled incandescent-heated fiber growth runs. The amplitude of persistent diameter variations was of the order of 10% of the fiber diameter. If significantly smaller, they damped out and if significantly larger, they amplified and finally caused the zone to neck off.

There is insufficient data to discuss the dimensional stability of the laser heated fibers quantitatively. Sections up to two inches in length were as good or better than the best incandescent filament grown fibers. With only a few exceptions, distortions in the feed rod caused the feed rod to drift out of the focal point of the optical system after two to three inches of growth. Once this occurred, the fiber surface was rough and irregular due to incomplete melting. It is reasonable to conclude that the dimensional quality of the laser heated fibers was nearly the same as those characterized in Table VI.

2. Surface Characteristic

The ambient atmosphere was found to have a significant effect on the smoothness of the fibers. The differences that were observed were attributed to the effects of gases coming out of solution at the solidifying interface.

When helium or vacuum atmospheres were used for fiber growth runs, bursting bubbles were observed on the surface of the zone. Occasionally, their effect was sufficient to cause the fiber to vibrate with an amplitude of approximately one diameter. Their effect was reduced by lowering growth rates although smooth surfaces were not achieved with either helium or vacuum atmospheres. Pulling in the downward direction also gave some improvement since bubbles burst adjacent to the melting interface rather than the freezing interface.

The fibers grown in an argon atmosphere at 1 psig (1.1×10^5 N/m^2) had the smoothest surfaces produced by incandescent heaters. Hydrogen and nitrogen gases or their mixtures could not be used with graphite heaters. The hydrogen produced a soot-like film; presumably by transporting carbon as methane.

When pure nitrogen atmospheres were used with graphite incandescent heaters, a equiaxed polycrystalline skin was produced on the fibers. The cause was not identified, but it must be more complex than a simple reaction with N_2 because the laser melted fibers, which were all grown in air, showed no evidence of a polycrystalline skin.

3. Porosity

Porosity was observed in varying concentrations and distributions, and in some cases approached zero concentration. Two distinct distributions of pores were observed which were oriented with respect to the fiber growth axis. In other cases, the pores were randomly distributed in the fiber. In all probability, the three distributions reflect differences in the solidification process; however, quantitative interpretation cannot be made at this time.

Figures 17 and 18 are longitudinal and axial sections of Fiber 23. Striation boundaries (lineage), pores concentrated in striation boundaries and a cellular network of the boundaries are evident in these two photomicrographs. These microstructural features are characteristic of cellular solidification interfaces in which the planar solidification interface breaks down to reduce the distance over which impurities must diffuse while the interface advances at a uniform rate. The boundaries contain relatively high impurity levels, and shrinkage cavities are likely to occur there since these are the last regions to solidify. Typically, there is a crystallographic misorientation across the boundaries. X-ray Laue photographs showed the misorientations to be less than one degree in this case.

Figure 19 shows Fiber 23 attached to the solidified zone from which it was grown. Macroscopically, the solidification interface is convex into the melt and is not faceted. This type of curvature promotes single crystal growth since spurious surface nuclei are rejected. It is not possible to confirm, on the basis of this photomacrograph, whether the solidification interface is in fact cellular as postulated; however, there do appear to be irregularities along the interface.

Many fibers exhibited a characteristic, regular distribution of pores which were concentrated in planes that extend diagonally across the fibers. A typical example is shown in Figure 20. The characteristic spacing and orientation of the planes varied from fiber to fiber and was not associated with any specific crystallographic plane. The spacing between planes of pores parallel to the fiber axis was quite uniform in many fibers over their

FIGURE 17 FIBER 23 SHOWING STRIATION BOUNDARIES AND PORES CONCENTRATED IN BOUNDARIES. FRONT ILLUMINATION 80x

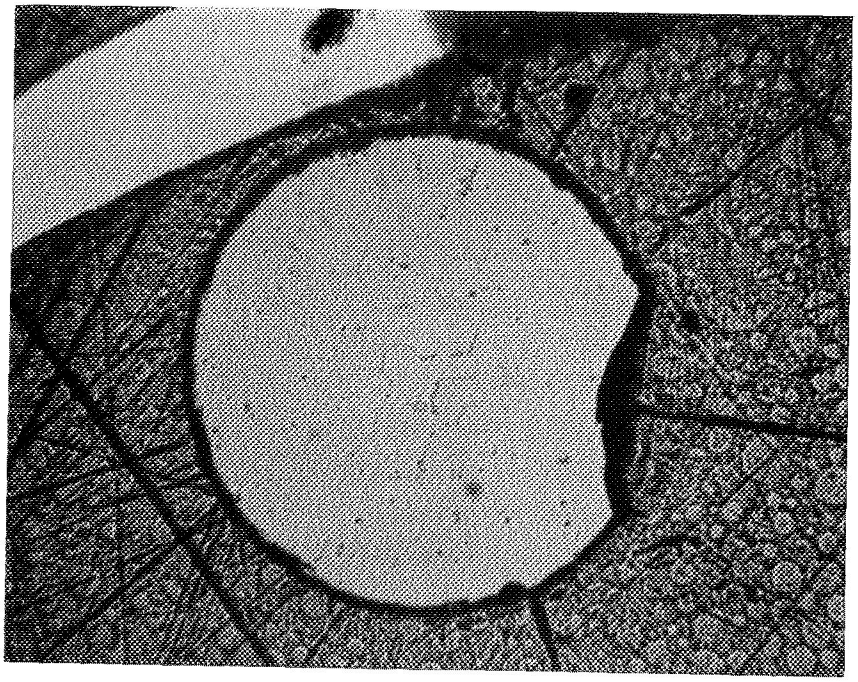

FIGURE 18 FIBER 23 SHOWING CELLULAR NETWORK OF STRIATION BOUNDARIES. FRONT ILLUMINATION 80x

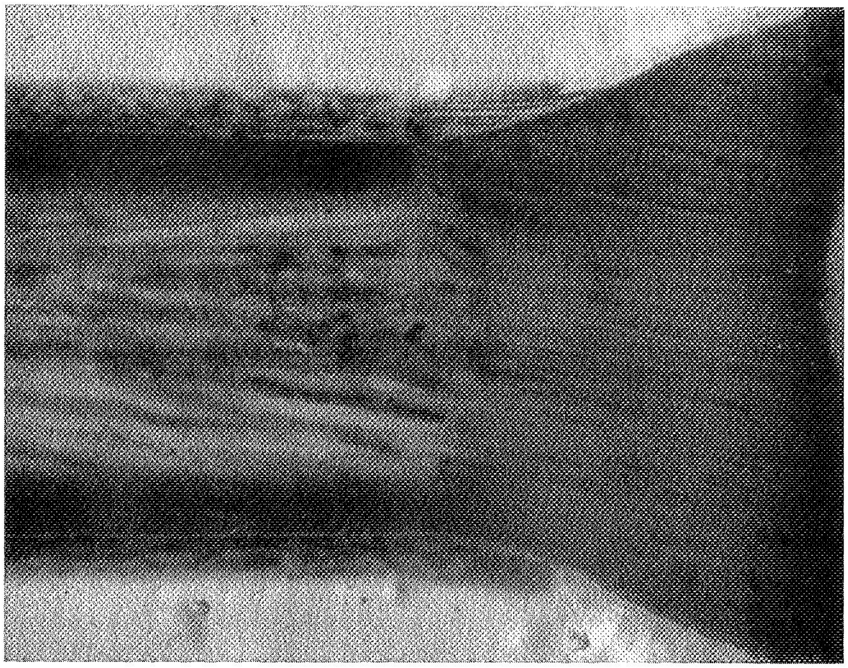

FIGURE 19 FIBER 23 ATTACHED TO SOLIDIFIED ZONE SHOWING SOLIDIFICATION INTERFACE. BACK ILLUMINATION 80x

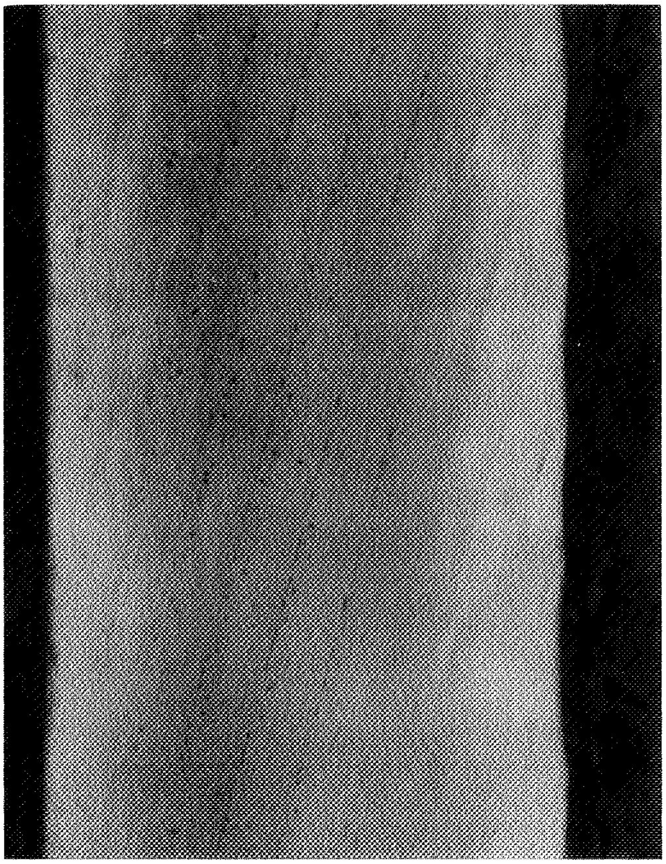

FIGURE 20 FIBER 1-h SHOWING CONCENTRATION OF PORES IN REGULAR PLANES. FRONT ILLUMINATION 137x

7 to 8 inch (17 to 20 cm) lengths. The distance between planes of pores along the fiber axis is of the order of 0.006 to 0.010 inch (0.0152 to 0.0254 cm). Pore sizes were approximately 80 micro inches (2×10^{-4} cm) in diameter and the characteristic distance between pores in the planes is in the range of 3 to 10 pore diameters.

In some cases, the surfaces of the fibers showed distinct discontinuities along the traces of the intersections between the fiber surfaces and the planes of pores. A particularly vivid example is shown in Figure 21. The discontinuities are also evident along the outside profile of Fiber 1-h in Figure 20. It appears reasonable to suspect that the causes of both the pores lying in well defined planes and the irregularities on the surfaces of the fiber may result from irregular, nonaxial motion of the fiber during growth. Porosity of this type is often observed along the contour of the solidification interface when it suddenly advances fast enough that the liquid becomes supersaturated with gas and the bubbles are entrapped by the advancing interface. If this is the case, fiber growth either does not take place in a direction parallel to the fiber axis or the growth interface is highly faceted. X-ray analyses have shown that unseeded growth axes vary and that the traces on the fiber surfaces do not correspond to specific crystallography planes. Neither is characteristic of faceted growth. Also, the solidification interface in Figure 19 did not show a growth facet. The only remaining explanation we have for the fiber morphology and pore structure is that the growth rate is irregular and that the actual direction of growth is not parallel to the fiber axis.

We were not able to confirm that this type of growth process was in fact operative. The zone and growing fiber were viewed under sufficient magnification that irregular, macroscopic motion of these dimensions and frequency should have been visible. None was observed with the exception of that induced by bursting bubbles. It is clearly important that the cause(s) for these regularly spaced planes be identified and eliminated since they will limit the strengths of the fibers to unacceptably low levels.

Other fibers were essentially free of pores and the few that remained were randomly distributed. Examples of these fibers are shown in Figure 22

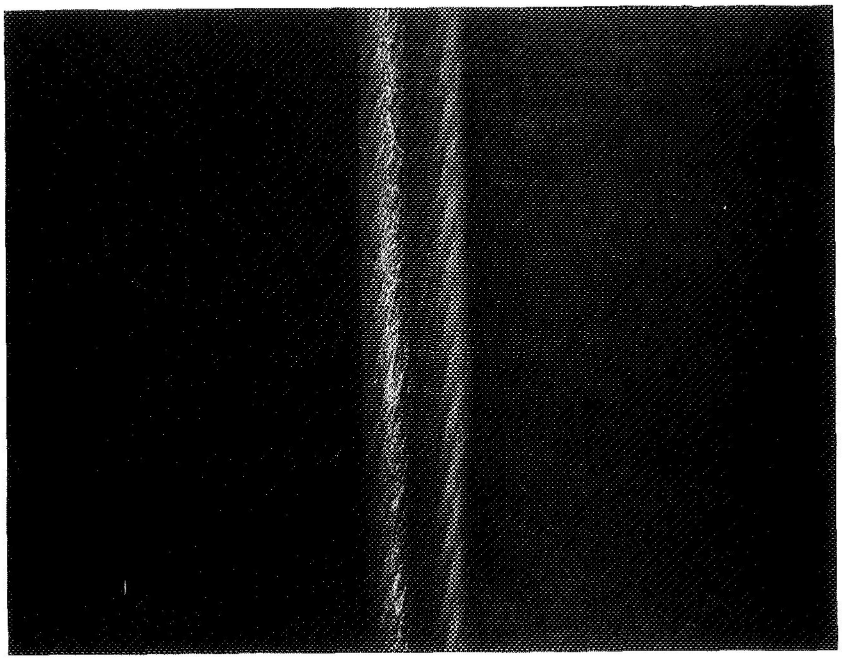

FIGURE 21 FIBER 1-h SHOWING EXTREME EXAMPLE OF SURFACE TEXTURE 32x

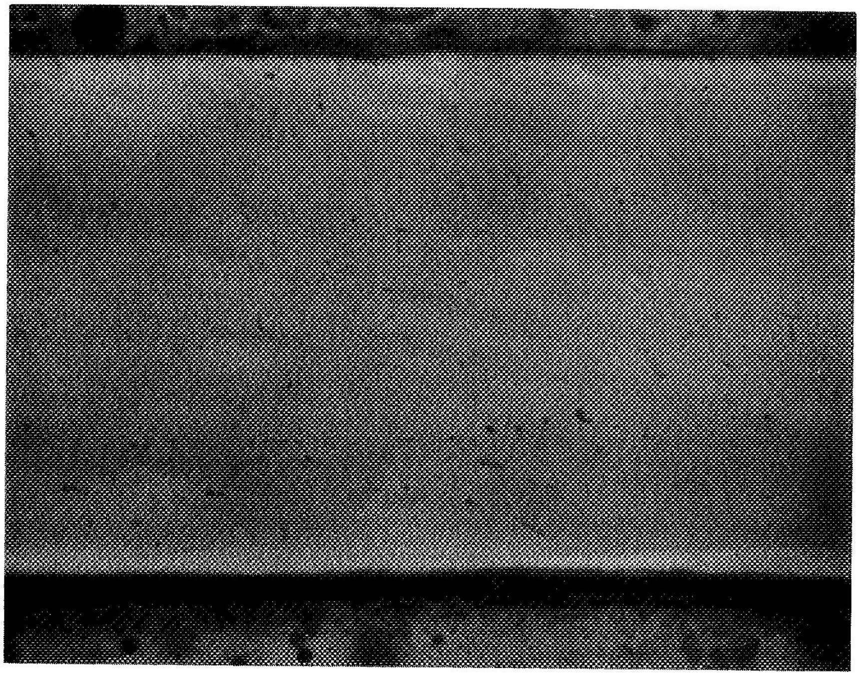

FIGURE 22 FIBER 1-j SHOWING RANDOM DISTRIBUTION OF PORES. FRONT ILLUMINATION 137x

and 23. Fiber 1-j (Figure 22) was nominally grown under the same process conditions as Fiber A-13 (Figures 20 and 21) yet the distribution of pores is quite dissimilar. Fibers 48 and 49 (Figure 23) were grown with the CO_2 laser heat source. These two fibers are free of pores in the sections photographed. The microstructural features in the two fibers are pores in the mounting material which are visible through the transparent fibers. The line of light extending the length of Fiber 48 results from light reflected from the surfaces of the fiber.

It is apparent from these photomicrographs that extremely high quality fibers can be produced by the floating zone fiber growth process. It is also apparent that much has to be learned about the factors which cause microstructural defects.

The differences between the measured diameter and the equivalent diameter based on a weight per unit length is a good measure of the diameter uniformity and porosity. This parameter is tabulated in the second to last column in Table VI. It can be seen that all of the equivalent diameters are smaller than measured diameters, and the differences are generally of the order of 0.0005 inch (0.00127 cm). If the entire difference between the two is attributed to internal porosity, the volume percent porosity is three times the percentage difference between the two diameters. (Last column in Table VI.) On this basis, porosities would range from 6 to 18.9%. Direct measurements of porosity from microstructural analyses indicate porosity levels in the range of 1%. The discrepancy is due to the fact that micrometer diameter measurements give the peak to peak distance. The differences between the measured diameter and the equivalent diameter is probably better measure of the long wavelength surface roughness than porosity.

C. X-Ray Characterization of Fibers

Fibers were subjected to X-ray Laue analysis to determine whether the fibers were single crystal, to gain a qualitative evaluation of crystal perfection and to determine growth directions.

All of the twenty fibers that were X-rayed were single crystal. Fibers which were initiated from polycrystalline feed rods generally were single crystal after growing several diameters in length. The progressive transition

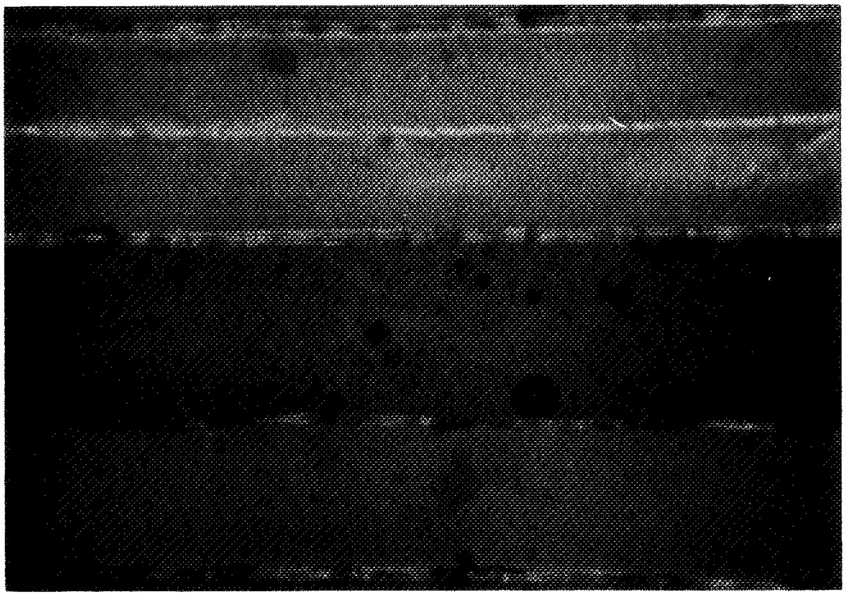

FIGURE 23 FIBERS 48 AND 49 SHOWING HIGHLY TRANSPARENT, PORE-FREE SECTIONS. FRONT ILLUMINATION 137x

from fine-grained polycrystalline to a single crystal fiber was readily visible to the eye. Both laser and incandescent heat sources had the same propensity to induce single crystal growth.

The degree to which diffraction spots split or smear is a qualitative measure of crystal perfection since the entire fiber cross section is imaged. The diffraction spots were generally sharp and their size was determined by the fiber diameter and the divergence of the diffracted X-ray beam. Occasional fibers showed misorientations across striation boundaries up to approximately 2°. Even these are considered good crystallographic quality for bulk single crystals.

The growth directions of all fibers grown prior to Batch 2 were uncontrolled. Growth was initiated either from polycrystalline feed rods or uncharacterized fibers from previous runs. No preferred growth directions were evident from X-ray Laue analyses of these fibers. This result is consistent with the observation that facets were not evident on the growth interface shown in Figure 19. Faceted growth tends to result in preferred growth directions.

Fibers grown in Batch 2 and all subsequent runs were initiated from TYCO fibers (supplied by the NASA Project Manager). These were nominally 0° fibers and X-ray analyses confirmed that the growth axes of two of the fibers used were in fact within 10° of the $\vec{c}$ axis. X-ray analyses of selected fibers from Batch 2 confirmed that the TYCO seeds had in fact established the growth axis in these fibers. X-ray analyses of fibers produced in subsequent batches showed the same random distribution of growth axes observed in fibers produced prior to Batch 2. Unfortunately, this result was discovered after all of the available TYCO fibers had been consumed, so it is not possible to state with certainty whether the seeding technique or the seeds were at fault. It is probable that sufficient time was not allowed to establish thermal equilibrium between the molten zone and the seed prior to initiating growth. This is one of the most common causes for uneffective seeding.

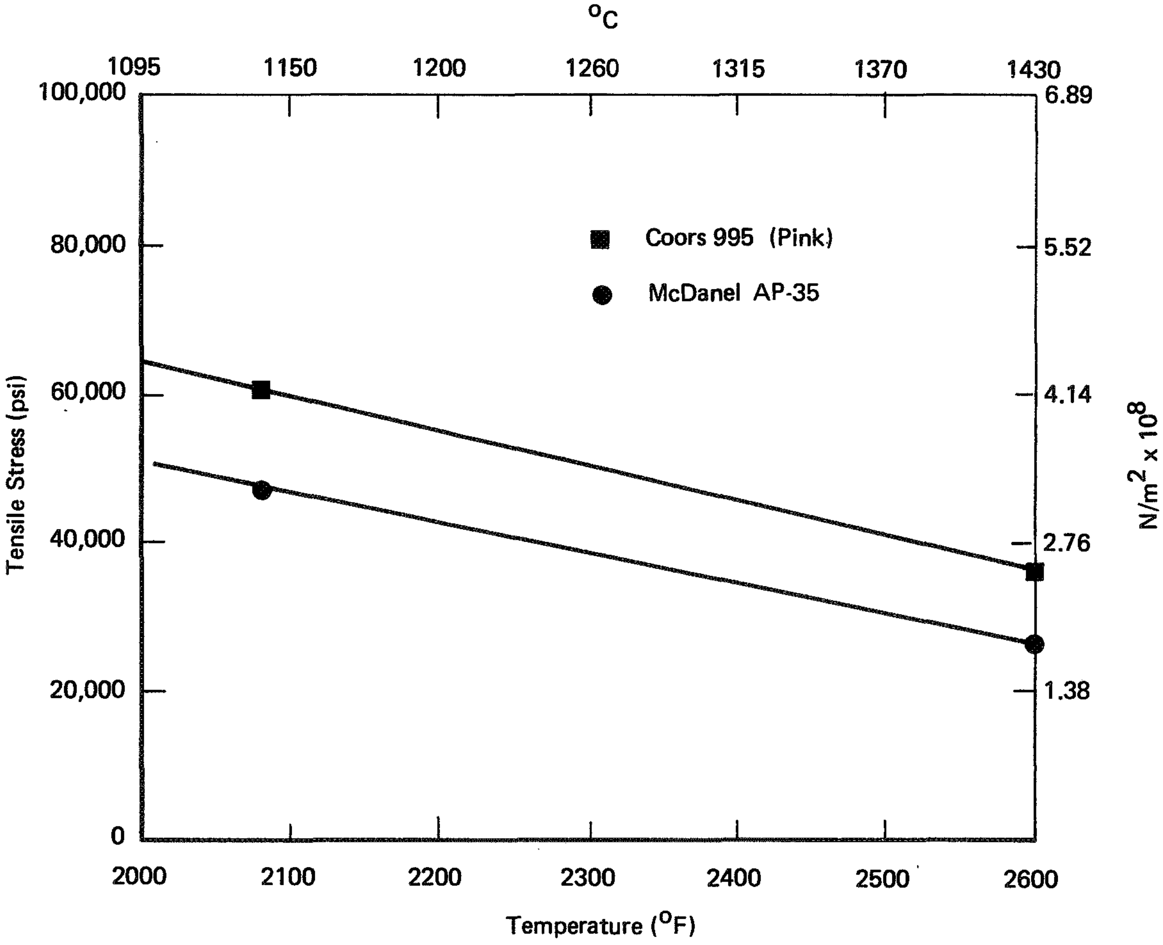

FIGURE 24 RESULTS OF HIGH TEMPERATURE TENSILE TESTS

D. Tensile Testing

1. Testing Technique

The fiber tensile specimens were mounted in slender members to minimize bending moments induced in the fibers by misalignment in the testing machine. These members consist of 0.050 inch (0.127 cm) diameter, 12 to 18 inch (30 to 45 cm) long pieces of music wire to which 0.75 inch (1.9 cm) long sections of hypodermic tubing have been brazed coaxially on one end. The tubing is slotted for approximately 0.5 inch (1.27 cm). Fibers are bonded to the two slender members with epoxy cement in a jig which aligns all three pieces coaxially. The maximum difference between the neutral axes of the music wires and that of the fiber was 0.015 inch (0.0381 cm) for the fiber tested to date. The gauge length was a minimum of 50 fiber diameters. The crosshead rate was 0.08 inch (0.2 cm) per minute.

2. Results of Room Temperature Tensile Tests

TABLE VII

ROOM TEMPERATURE TENSILE STRENGTHS

Batch	No. Tests	Average Strength		Standard Deviation
		psi x 10^3	N/m^2 x 10^8	
1	15	74	5.10	42%
2	9	98	6.76	45%
3	4	86	5.93	40%
4	6	77	5.31	73%
5	5	116	8.00	11%
6	9	101	6.96	26%
7	5	114	7.86	7%
Laser*	10	59	4.07	37%

The maximum tensile strength observed was 175,000 psi (12.06 x 10^8N/m^2) (Batch 4), and the lowest was 23,000 psi (1.59 x 10^8N/m^2) (Batch 2). In Batch 1 seven pairs of samples were taken from tops and bottoms of fibers

---

*Fibers 43, 44, 45, 46, 48, 49, 52, 53, 54, 57.

for comparisons. With one exception all of the tops were slightly stronger, but the differences between the averages [top = 73,962 psi (5.1 x $10^8 N/m^2$); bottom = 73,785 psi (5.09 x $10^8 N/m^2$)] was negligible. All other samples were taken from the bottoms of fibers. Generally, it was not possible to determine whether the fibers broke away from the grips because they shattered into many pieces.

Two TYCO fibers were tested by the same technique to determine whether the testing procedure gave valid results. One broke at a grip at an apparent tensile strength of 21,000 psi (1.45 x $10^8 N/m^2$) and the other away from the grip at a tensile strength of 169,000 psi (1.17 x $10^8 N/m^2$). To further clarify whether the testing technique was responsible for the relatively low strengths, the Project Manager tested a number of TYCO fibers from the same batch at room temperature. These strengths ranged from 185,000 to 200,000 psi (12.76 - 13.79 x 10^8 N/m^2). He also tested ADL fibers from Batch 1 and observed tensile strengths of approximately 95,000 psi (6.55 x $10^8 N/m^2$) compared with 74,000 psi (5.10 x $10^8 N/m^2$) measured at ADL. The ratio between both sets of results is approximately 1.3 so it appears that a bending stress was introduced by this tensile testing procedure.

Based on the microstructures that have been analyzed, no realistic correlation can be made between porosity and tensile strengths. Fiber 1-h (Figure 20) broke at 72,000 psi (4.96 x $10^8 N/m^2$), Fiber 1-j (Figure 22) at 47,000 psi (3.24 x $10^8 N/m^2$), Number 47 and 48 (Figure 23) which are virtually porefree at 60,800 psi (4.19 x $10^8 N/m^2$) and at 82,500 psi (5.69 x $10^8 N/m^2$) respectively. Many of the fibers which exhibited tensile strengths in excess of 100,000 psi (6.89 x $10^8 N/m^2$) had pores concentrated in planes similar to those shown in Figure 20.

It seems reasonable to conclude on the basis of these results that the strengths are limited by surface defects rather than existing bulk defects. Further evidence to support this conclusion is that fracture surfaces did not follow planes of pores. It also should be noted that while the laser melted fibers were glassy smooth over lengths of several diameters, individual sharp defects were observed on surfaces of most of these fibers. All of the fibers grown during the program, as well as the

TYCO fibers which were made available, were freely handled prior to testing. No precautions were taken to prevent abrasion so surface damage should be suspected.

3. Results of Elevated Temperature Tensile Tests

Fibers from Batches 14, 15, 16, and 17 were tensile tested at elevated temperatures. The samples were gripped in the same manner used for room temperature tests except that 4 inch (10 cm) lengths were used to remove the epoxy joints from the heat. The furnace consisted of an internally wound platinum furnace insulated by high purity BN backed with fibrous mullite. Two furnaces were used during the high temperature testing. The indicated temperature was compared to the maximum temperature within the cavity of the first and found to agree within 20°F (11°C). This comparison was not made in the second until the testing was completed and the temperature differences were found to be 80°F (45°C) at 2000°F (1095°C) and 200°F (110°C) at 2400°F (1320°C). The actual test temperatures were 2080 and 2600°F (1140 and 1430°C). The average measured strengths are plotted in Figure 24 as a function of temperature. The lines connecting corresponding points are for purposes of interpolation only. The highest strength measured at 2080°F (1140°C) was 72,000 psi ($4.96 \times 10^8 N/m^2$) for Coors 995 (pink). Room temperature tensile strengths for the 4 inch (10 cm) tensile specimen were 112,500 and 96,700 psi (7.72 and $6.67 \times 10^8 N/m^2$) respectively for McDanel's AP-35 and Coors 995 (pink). These are within one standard deviation of the strengths reported in Table VII for one inch gauge length specimens.

The results of the high temperature tensile tests are consistent with the results of our room temperature measurements. Other measurements have shown that Al_2O_3 fiber tensile strengths at 2000°F (1095°C) drop by a factor of approximately four from those observed at room temperature.(5) In this case, the drop was more nearly a factor of two; however, the data is extremely limited in both cases. The chromium doped materials (Coors 995 (pink)) is consistently stronger than high purity McDanel AP-35 at elevated temperatures. This may result from reduced dislocation mobility; however, substantiation of the conclusion requires additional experimentation.

VI. SUMMARY OF RESULTS

During this program single crystal sapphire fibers have been grown by a floating zone technique conceived by Arthur D. Little, Inc.

The detailed shapes of small molten zones between different size solid rods was analyzed for the first time. The limits of absolute stability were defined and metastable limits were defined for specific examples. A kinematic analysis showed for the first time that the tangent of the molten zone at the solidifying interface tends to be parallel to the direction of growth. This feature is important for maximizing dimensional uniformity. It was also shown that perturbations from the steady state zone volume tend to drop out rapidly if the zone height remains constant.

Possible heat sources for the floating zone fiber growth process were assessed in terms of list of criteria that were felt important. Incandescent filament and CO_2 laser heat sources were identified as the best. The incandescent heaters had temperature restrictive limitations but were felt to be the most amenable to multi-fiber growth processes. CO_2 laser heat sources combine a number of features which make them highly attractive for an exploratory program for high temperature fibers.

On the basis of these analyses, fiber growth experiments were initiated with both types of heaters. Pyrolytic graphite was found to be the best material for incandescent heaters, both when rf heated and conventionally resistance heated. A leased 10 watt CO_2 laser was used to demonstrate the feasibility of using this heat source for the fiber growth process. Both heating techniques performed as well as anticipated on the basis of the analyses.

The quality of fibers which were produced were shown to be highly sensitive to feed rod materials, atmosphere, and physical process conditions. Pore-free and highly uniform fibers were produced under limited, but well defined, conditions.

The surface roughnesses were not quantitatively described nor were fibers treated to avoid or eliminate surface defects. It is suspected that the strengths, which are somewhat lower than others reported for sapphire single crystals, are limited by surface defects. This conclusion is consistent with other reported strengths and fiber treatments. It is suspected that a bending stress was induced in the fibers during the "tensile" tests which also lowered the apparent strengths.

Tensile strengths up to 72,000 psi (4.96×10^8 N/m^2) were measured at 2080°F (1140°C) with chromium doped Al_2O_3 fibers. These results are consistent with room temperature strengths but are lower than the program's goal [100,000 psi (6.9×10^8 N/m^2) at 2000°F (1095°C)].

All of the goals of the program were met within the time schedules and funding limits proposed, with the exception of the high temperature tensile strengths. This probably resulted from surface defects which limited room temperature strengths. The effect of their elimination has been demonstrated by others and post-growth surface treatments explicitly were not included in this program.

ACKNOWLEDGMENTS

The authors received assistance from several Arthur D. Little, Inc., staff members while conducting this program. Dr. A. Emslie and Mr. P. Strong conducted the zone shape and stability analysis, Drs. A. Wechsler and A. Sarofim (M.I.T.) conducted the thermal analysis, Mr. J. Wenckus assisted in design of the fiber growth apparatus, Mr. P. VonThuna and Mr. L. Lapson designed the optics used for the CO_2 laser heated experiments, and Mr. L. Lindonen was responsible for carrying out most of the latter fiber growth experiments.

Their assistance and contributions are gratefully acknowledged.

REFERENCES

1. Robert F. Green, "Governing Equations for the Shapes of Molten Zones," J. Appl. Phys. 35, 1297 (1967).
2. D. W. Lee and W. D. Kingery, "Radiation Energy Transfer and Thermal Conductivity of Ceramic Oxides," J. Am. Ceram. Soc. 42, 594-607 (1960).
3. D. B. Gasson and B. Cockayne, "Oxide Crystal Growth Using Gas Lasers," J. Mat. Sci. 5, 100 (1970).
4. K. Eickhoff and K. Biurs, "Tiegelfreies Zonenschmelzen von Rubinkristalleu Durch Aufheizen Der Schmelzzone Mittels Laser," J. Crys. Gr. 6, 21 (1969).
5. M. J. Noone, "Development of Composite Materials for High Temperature Applications," Final Report N000 19-69-C-0310.

DISTRIBUTION LIST

(The number in parentheses is the number of copies sent to each addressee.)

NASA Headquarters
600 Independence Avenue
Washington, D. C. 20546
Attn: N. F. Rekos (RAP) (1)
G. C. Deutsch (RR-1) (1)
R. H. Raring (RRM) (1)
J. J. Gangler (RRM) (1)

NASA-Lewis Research Center
21000 Brookpark Road
Cleveland, Ohio 44135
Attn: Technology Utilization Office, MS 3-19 (1)
John Weeton, MS 49-1 (1)
G. M. Ault, MS 3-13 (1)
R. W. Hall, MS 105-1 (1)
Library, MS 60-3 (2)
Report Control Office, MS 5-5 (1)
H. B. Probst, MS 49-1 (1)
R. A. Signorelli, MS 106-1 (1)
L. J. Westfall, MS 106-1 (22)
A. E. Anglin, MS 106-1 (1)
L. W. Shopen MS 77-3 (1)

FAA Headquarters
800 Independence Avenue, SW
Washington, D. C. 20553
Attn: Brig. Gen. J. C. Maxwell (1)

NASA Scientific and Technical Information Facility (6)
P. O. Box 33
College Park, Maryland 20740

U. S. Atomic Energy Commission
Washington, D. C. 20545
Attn: Technical Reports Library (1)
Jules Simmons (1)

Air Force Office of Scientific Research (1)
Propulsion Research Division
USAF Washington, D. C. 20525

Defense Documentation Center (DDC) (1)
Cameron Station
5010 Duke Street
Alexandria, Virginia 22314

Headquarters
Wright-Patterson AFB, Ohio 45433
Attn: MAAM-Technical Library (1)
AFSC-FTDC (1)
AFML-A. M. Lovelace (1)
SESOS (1)

Department of the Navy
ONR
Code 429
Washington, D. C. 20525
Attn: Dr. R. Roberts (1)

U. S. Army Aviation Materials Laboratory
Fort Eustis, Virginia 23604
Attn: John White, Chief, SMOFE-APG (1)

Chief, Bureau of Naval Weapons
Department of the Navy
Washington, D. C. 20525
Attn: T. F. Kearns (1)

NASA-Langley Research Center
Langley Field, Virginia 23365
Attn: Library (1)
Richard Pride (1)

NASA-Marshall Space Flight Center
Huntsville, Alabama 35812
Attn: Library (1)

Jet Propulsion Laboratory
4800 Oak Grove Drive
Pasadena, California 91102
Attn: Library (1)

Army Materials Research Agency
Watertown Arsenal
Watertown, Massachusetts 02172
Attn: S. V. Arnold, Director (1)

NASA-Ames Research Center
Moffett Field, California 94035

NASA-Goddard Space Flight Center
Greenbelt, Maryland 20771
Attn: Library (1)

NASA-Manned Space Flight Center
Houston, Texas 77058
Attn: Library (1)

NASA-Flight Research Center
P. O. Box 273
Edwards, California 93523
Attn: Library (1)

Defense Metals Information Center
  (DMIC) (1)
Battelle Memorial Institute
505 King Avenue
Columbus, Ohio 43201

General Electric Company
Advanced Technology Laboratory
Schenectady, New York 12305
Attn: Library (1)

General Electric Company
Materials Development Laboratory
  Operation
Advanced Engine and Technology
  Department
Cincinnati, Ohio 45215
Attn: L. P. Jahnke (1)

General Motors Corporation
Allison Division
Indianapolis, Indian 46206
Attn: D. K. Hanink, Materials
  Laboratory (1)

Stanford University
Palo Alto, California 94305
Attn: Prof. Oleg Sherby, Dept.
  of Mat'l Science (1)

United Aircraft Corporation
400 Main Street
East Hartford, Connecticut 06108
Attn: E. F. Bradley, Chief,
  Mat'l Eng. (1)

United Aircraft Corporation
Hamilton Standard Division
Windsor Locks, Connecticut 06096
Attn: H. P. Berie (1)

Lockheed Mississippi Space Co.
Palo Alto Research Lab
Palo Alto, California
Attn: J. L. Camahort (1)

Lockheed-Georgia
Dept. 72-14
Marietta, Georgia 30060
Attn: Dr. W. Cremens, Zone 402 (1)

Clevite Corporation
7000 St. Clair Avenue, N.E.
Cleveland, Ohio 44110
Attn: G. F. Davies (1)

Maggs Research Center
Watervliet Arsenal
Watervliet, New York 12189
Attn: Dr. I. Ahmad

NASA-Langley Research Center
Langley Station
Hampton, Virginia 23365
Attn: John Buckley (1)

General Electric AETD
Evandale, Ohio 45215
Attn: Dr. W. H. Chang (1)

L. W. Davis (1)
Harvey Engineering Labs
Harvey Aluminum Co.
19200 S. Western Avenue
Torrance, California 90509

J. Bartos (1)
General Electric AETD
Evandale, Ohio 45215

C. A. Calow (1)
U. K. A. E. A.
Atomic Weap. Research Est.
Aldermaston, Berkshire
England

W. A. Compton (1)
Solar Division Int. Harvester
2200 Pacific Highway
San Diego, California

Dr. D. Cratchley (1)
Rolls-Royce Ltd.
The Old Hall
Littleover, Derby
England

Dr. M. A. Decrescente (1)
Chief, High Temp. Mat.
United Aircraft Research Lab.
East Hartford, Connecticut 06108

Dr. F. S. Galasso (1)
Chief, Mat. Syn. Sec.
United Aircraft Research Lab.
East Hartford, Connecticut 06108

G. C. Grimes (1)
Southwest Research Ins.
8500 Culebra Road
San Antonio, Texas 78206

Dr. M. Ferman (1)
Allison Division, GMC
Department 5827
P. O. Box 894
Indianapolis, Indiana 46206

Dr. L. M. Gillin (1)
Aeronautical Research Labs
G. P. O. Box 4331
Melbourne, C. 1
Victoria, Australia

K. R. Hanby (1)
Battelle Memorial Institute
505 King Avenue
Columbus, Ohio 43201

H. Herring (1)
NASA-Langley Research Center
Structure Research Division
Langley Station
Hampton, Virginia 23365

Dr. A. Kelly (1)
Superintendent
Div. Inorg/Metallic Str.
Nat. Physical Laboratory
Teddington, Middlesex
England

Dr. H. G. Kreider (1)
United Aircraft Research Lab.
East Hartford, Connecticut 06108

Professor Tsuyoshi Hayashi (1)
Structures Research Institute
University of Tokyo
Hongo 7-3-1, Bunkyo-Ku
Tokyo, Japan

Major Jon Kershaw (1)
MAMS
Wright Patterson Air Force Base
Ohio 45304

Dr. R. H. Krock (1)
P. R. Mallory Co.
Northwest Industrial Park
Burlington, Massachusetts 01803

D. P. Laverty (1)
Section Mgr., Mat. Tech.
Equip. Labs. Div. of TRW
23555 Euclid Avenue
Cleveland, Ohio 44117

Dr. E. M. Lenoe (1)
Avco Corporation
Lowell Industrial Park
Lowell, Massachusetts 01850

Dr. S. R. Lyon (1)
AFML (MAMS)
Wright-Patterson Air Force Base
Ohio 45304

Dr. A. G. Metcalfe (1)
Solar Division
Int. Harvester Co.
2200 Pacific Highway
San Diego, California

A. Lawley (1)
Drexel Institute of Technology
Dept. of Metals Engineering
32 and Chestnut Streets
Philadelphia, Pennsylvania 19104

A. P. Levitt (1)
Army Mat./Mech. Research
Watertown, Massachusetts 02172

L. McCreight (1)
General Electric Co.
Valley Forge Space Technology
P. O. Box 8555
Philadelphia, Pennsylvania 19101

Dr. Ishi Miura (1)
Tokyo Medical/Dental University
1-Chome
Yushima Bunkyo-Ku
Tokyo, Japan

M. C. Nicholas (1)
Atomic Energy Research Est.
Harwell, Berkshire
England

Librarian, Lycoming Division (1)
AVCO Corp.
550 South Main Street
Stratford, Connecticut 06497

G. D. Menke (1)
Honeywell, Inc.
Minneapolis, Minnesota 55400

R. G. Moss (1)
Jet Propulsion Lab.
4800 Oak Grove Road
Pasadena, California 91103

Technical Librarian (1)
North American-Rockwell
4300 E. 5th Avenue
Columbus, Ohio 43216

Dr. M. J. Salkind (1)
United Aircraft Corp.
Sikorsky Aircraft Division
Stratford, Connecticut 06497

Capt. W. A. Schulz (1)
AFMU
Wright-Patterson AFB
Ohio 45304

J. C. Weithers (1)
General Technical Corp.
1821 Michael Faraday Drive
Reston, Virginia 22070

R. T. Pepper (1)
Aerospace Corp.
Building H1, MS 2281
P. O. Box 95085
Los Angeles, California 90045

H. Shimizu (1)
Marquardt Corp.
16555 Saticoy Street
Van Nuys, California 91409

A. Toy (1)
Material Sciences Dept.
TRW Systems Group
One Space Park
Redondo Beach, California 90278

W. Wolkowitz (1)
Crumman Aircraft Eng.
Bethpage, Long Island
New York 11714

R. K. Robinson (1)
Ceramics/Composites Division
Battelle-Northwest
3000 Stevens Drive
Richland, Washington 99352

Professor E. Scala (1)
Bard Hall
Cornell University
Ithaca, New York 14850

Dr. D. M. Schuster (1)
Sandia Corporation
Metallurgy Division 5431
P. O. Box 5800
Albuquerque, New Mexico 87115

B. A. Wilcox (1)
Metal Science Group
Battelle Memorial Institute
505 King Street
Columbus, Ohio 43201

Dr. G. Wirth (1)
DFVLR
Institut Fur Werkstoff-Forschung
505 Porz-Wahn
Linder-Hohe, Germany

A. J. Yeast (1)
Space Division
North American-Rockwell
12214 Lakewood Boulevard
Downey, California 90241

William G. Jurevic
Advanced Composites Information
Center
Lockheed-Georgia Company
D/72 Zone 402
Marietta, Georgia 30060

Jack H. Ross (1)
AFML (Fibrous Materials Branch)
Wright-Patterson Air Force Base
Ohio 45433

Owens-Corning Fiberglas Corporation
Technical Center
Granville, Ohio 43023
Attn: Miss B. J. Nethers, Librarian

Rutgers University (1)
School of Ceramics
University Heights Campus
New Brunswick, New Jersey 08903
Attn: Professor W. H. Bover

United Aircraft Corporation (1)
Pratt & Whitney Division
West Palm Beach, Florida 33402
Attn: Library

R. E. Tressler (1)
MAMS Metals and Ceramics Division
Wright-Patterson Air Force Base
Ohio 45304